Universitat Politècnica de Catalunya
Master of Science in Computational Mechanics

Departament de Matemàtica Aplicada III

3D Mixed mode constitutive damage evolution model for composite materials

by

Sujith V Sukumaran

This thesis is submitted in partial fulfillment of the requirement for the Degree of Master of Science in Computational Mechanics under the Erasmus Mundus programme, by University of Swansea, UK and Universitat Politècnica de Catalunya, Spain

Master Thesis

Advisors: Dr. Jose Muñoz
and
Dr. J.L. Curiel Sosa

Barcelona, June 21, 2010

3D Mixed mode constitutive damage evolution model for composite materials

Sujith V Sukumaran, Universitat Politècnica de Catalunya

In this thesis a 3D constitutive model is presented for the numerical prediction of unidirectional composite material behaviour under impact loading. The heterogeneous nature of composite materials gives rise to complex failure behaviour presenting itself in various failure modes. Impact loading usually results in complex three dimensional stress states which significantly influence the failure behaviour. In order to capture such failure behaviour, physically based three dimensional theories are required which predict the onset and evolution of the failure modes based on damage detection criteria and subsequent growth. Further, the distinct strain rate dependent behaviour due to the use of the polymeric matrices in composites needs to be incorporated in the constitutive models applied in numerical simulation of impact events.

The presented constitutive model relies on the prediction of damage detection by using physically based three dimensional stress based failure criteria. Damage evolution is predicted by incorporating a theoretical strain rate dependent damage model. The dissipation potential considers only those stress terms that directly contribute to the occurrence of a particular failure mode. The stiffnesses corresponding to these stress terms are degraded thus simulating damage evolution. The mesh dependency effects attributed to Continuum Damage Mechanics formulation is reduced to some extent by using a ply based modelling strategy, however, the constitutive equations themselves do not incorporate any element size dependent parameter.

The presented constitutive model is verified by numerically simulating aerospace industry standard impact experiments at different impact energies. The capability of the model to detect delamination damage presented in the experimental results is

demonstrated. Good qualitative comparisons were obtained with certain shortcomings in the quantitative results. However, a significant improvement was obtained towards the development of the model.

Acknowledgments

I would like to begin my acknowledgements by thanking my supervisors Dr. Jose Muñoz and Dr. J. L. Curiel Sosa. Thank you Dr. Muñoz for taking out time to discuss, review and suggest improvements towards the completion of the thesis tasks. Every time I came knocking on your doors, you provided me with valuable inputs to keep moving forward. To Dr. Curiel, thank you for presenting me with an opportunity to explore this topic and providing necessary literature to gain understanding of the topic. Thank you both for all the patience and guidance you provided me over the course of this thesis.

It was a matter of great pride to be part of the select group of Erasmus Mundus students undergoing this programme. Studying in this programme was a challenging and enriching experience. Thank you to all the educators at Swansea and UPC who taught us advanced topics in numerical methods. Thank you to all my colleagues from whom I learned a great deal in the past 2 years. The exchange of ideas and opportunities to discuss and learn the unknown was a constant source of inspiration. I would like to specially mention Hannes, Sebastien and Cesar, who have contributed to my learning a great deal. My first ever attempt at using LaTeX through this document would not have been possible without the initial introduction by Hannes.

I kindly acknowledge the financial support by means of scholarship of EU to undergo this masters programme. Without the administrative support from Lelia at UPC, the integration into the programme and at Barcelona would not have been so easy. Thank you for always being there to provide help.

My acknowledgements would be incomplete without a mention of my former managers at `TIMKEN`, Brad and Craig, who continue to be my motivators and philosophers. Finally, I would like to thank my family, in-laws and my wife Souparnika who always encouraged me to complete the programme even though this meant not having me

around. In between the rigours of the programme, it was a welcome break and a source of strength to be able to visit home and spend time with you.

Contents

List of Figures

Chapter 1

Introduction

1.1 Motivation and Background

In today's world, conventional metallic materials and their derivatives continue to be developed, applied and improved to offer ever increasing performance in myriad applications, including aerospace structures. They have a fundamental role to play in these applications, however, the ever increasing demand for lighter structures is continually resulting in replacement of metal parts by composite structures. This is particularly true of the aerospace industry, where the considerable benefits offered by composites are yet to be fully exploited but are already showing an increase in efficiency without compromise of safety. Composite materials are particularly attractive to aerospace applications because of their exceptional strength and stiffness-to-density ratios and superior physical properties.

Initially composite materials were used only in secondary structures in aircrafts, but as knowledge and development of the materials has improved, their use in primary structures such as wings and fuselage has increased (Quilter, 2008). The B2 stealth bomber is an interesting case. The requirement of radar-absorbing material on the exterior of the aircraft came with additional weight penalty. Composites were therefore used in the primary structure to offset this penalty. Among the first uses of

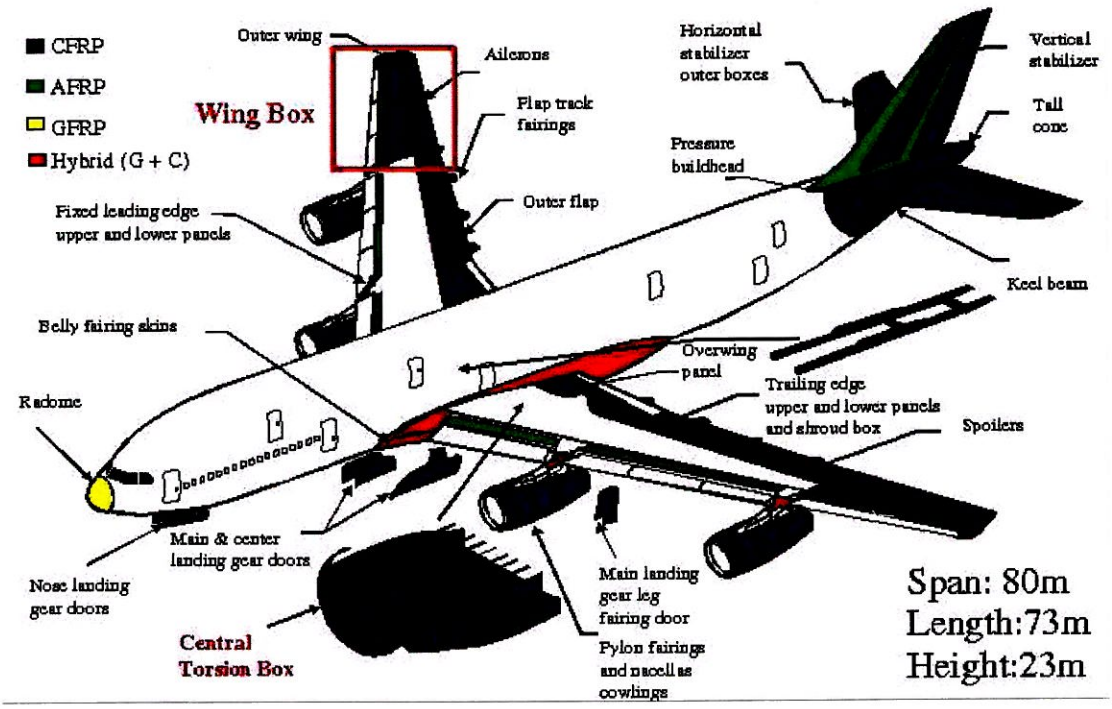

Figure 1.1: Carbon Fibre Reinforced Polymer (CFRP) parts in the new Airbus A380 (After http://www.msm.cam.ac.uk)

the modern composite materials was about 30-40 years ago with the usage of boron-reinforced epoxy composites for the skins of the empennages (tail section) of U.S. military aircrafts. The applications of composites, until recently, were mainly limited to the military where extensive testing programs could be undertaken. A lack of confidence for safe design, high cost of material and manufacturing and limited technology readiness had necessitated such testing programs. However, with an increase in understanding of the material behavior and decline in prices, the application of composites in civil aviation is at an all time high and expected to continually grow. The newest testament to this fact is the substitution of metallic components by hybrid or composite materials in the new Airbus A380 passenger plane (Fig. 1.1). The use of composite materials in commercial transport aircraft is attractive because reduced airframe weight enables better fuel economy and therefore lower operating costs.

With the increased usage in civil aerospace applications, comes the need for reliable and cost efficient design tools. The damage modes strongly influence the residual strength and thus the certification procedures. The industry uses conservative strain limited design rules to determine the safe loads. However, numerical analysis tools like Finite Elements (FE) with realistic constitutive models, can enhance performance and safety by more sophisticated structural design and at the same time, decrease the development costs and time as experimental design verification can be significantly reduced.

Among the various structural design considerations, impact events appear as a critical loading event. They pose several difficulties for design due to the development of complex three-dimensional stress states in such cases. This requires advanced theories for strength and damage prediction. Furthermore, composite materials, especially with polymeric matrices, are well known for their strain rate dependent material behavior. As a consequence, special constitutive models for the numerical simulation of impact events are required.

The current predictive capability of composite constitutive models is often limited in comparison to what is needed to master the above challenges (Weigand, 2009). A majority of the available models are limited to plane stress and representation of complex composite behavior often lacks sound physical basis. Only very recently, physically-based three dimensional failure theories have started to emerge. These novel theories aim at representation of failure mechanisms and enable a more realistic prediction of the various composite failure modes. Constitutive models incorporating strain rate dependent material behavior enable a realistic progressive damage growth prediction induced by impact loading.

1.2 Objectives

The primary driving force behind this research work was a motivation to contribute in a limited way to the overall goal of introducing composite materials in parts of an aircraft such as the engine blades that face serious risk of damage by means of an impact event. Within the scope of this body of work, a contribution is made to enhance the predictive capabilities of existing constitutive models for unidirectionally reinforced continuous Carbon Fibre Reinforced Polymers (CFRP) subject to impact events. The constitutive model used is developed for explicit FE which has demonstrated to be a powerful tool for the simulation of impact events. The following specific tasks are addressed within the thesis:

- *selection/extension of physically based failure theories which enable improved prediction of the onset of damage*
- *incorporation of strain rate dependent material behavior into the constitutive equations and propagation of damage evolution*
- *implementation of the resultant constitutive model into an explicit FE environment*
- *verification of the model by simulation of practically conducted experiments*

To perform the above tasks, an existing theoretical strain rate dependent evolution model is proposed to be combined with chosen physically based failure theories from literature for prediction of damage initiation and subsequent damage evolution. The resultant model, provided as an external user defined subroutine in an explicit FE environment, can be applied to a physical model representing practical experimental test(s). The results from the simulation of such test(s) will help verify the

constitutive model and suggest improvements in the formulation. Though a similar effort was undertaken previously, the model definition was found to be erroneous rendering the obtained results inconclusive and non-admissible. In the present work, careful consideration is given to all modelling aspects to provide original substantial contribution towards the overall research theme. No experimental work is undertaken in this research due to the limited scope, however, the simulation results will pave a way for better application of an inverse modelling approach with the model, whenever attempted in the future.

1.3 Brief Introduction to Composite Materials

Composites form one of the four basic categories of structural materials; the others being, *metals*, *polymers* and *ceramics*. A composite material is defined as one consisting of two or more separate materials combined in a macroscopic structural unit to form a third useful material. Thus, a composite is *heterogeneous*. A well designed composite material can usually exhibit the best qualities of the constituents and often some qualities that neither constituent possesses. They can be *engineered* to meet the specific demands of each particular application, thus providing an additional 'degree of freedom' during the design of a structure.

Composite materials are typically composed of a reinforcing material and a matrix material. Based on the type of reinforcing material, the composite can be categorized as a fibrous composite material or particulate composite. Wood and bone are natural composite materials: wood consists of cellulose fibres in a lignin matrix (see Fig. 1.2) and bone consists of hydroxyapatite particles in a collagen matrix. Carbon- and Glass-Fibre-Reinforced Polymers (CFRP and GFRP), which consist of carbon and glass fibres respectively, are the better known man-made composite materials belonging to the category of fibrous composite materials that are widely used in the aerospace and other industries. Metal matrix composites (MMC) currently being developed for the aerospace industry are examples of particulate composites and consist, usually,

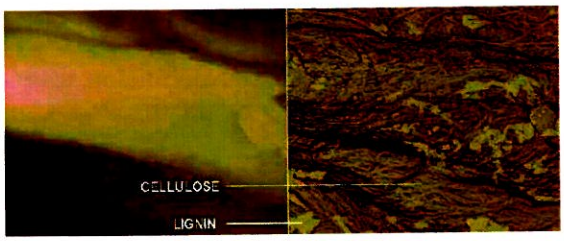

Figure 1.2: Constituents in wood (http://www.asmicro.com)

of non-metallic particles in a metallic matrix; for instance silicon carbide particles combined with aluminum alloy (Quilter, 2008).

The fibres in CFRP and GFRP are stiff and strong (for their density), but brittle, in a polymer matrix, which is tough but neither particularly stiff nor strong. The fibres in this combination give the material outstanding strength and stiffness with the matrix allowing for the force transmission between the fibres. Additionally, the matrix protects the fibre and keeps the composite together. The selection of specific fibre and matrix to be used in a composite is not arbitrary. The composite generally must be resistant to debonding at the fibre/matrix interface, and it must also be resistant to fibre breakage and matrix cracking. However, in applications such as crash or impact, where it is desirable to dissipate energy during the failure process, progressive fibre failure and fibre/matrix debonding are considered as positive features.

Probably one of the single most striking difference between fibrous and particulate composites, and indeed between fibrous composites and conventional metallic materials, relates to directionality of properties. Particulate composites and conventional metallic materials are isotropic, i.e., their properties (strength, stiffness, etc.) are the same in all directions; fibrous composites are anisotropic, i.e., their properties vary depending on the direction of the load with respect to the orientation of the fibres. This anisotropy is overcome by stacking layers, each often only fractions of millimetre thick, on top of one another with fibres oriented at different angles to form a *laminate*. The individual layers are referred to as *ply* or *lamina*. A single lamina with only one orientation of the fibres is called unidirectionally (UD) reinforced. In most aerospace

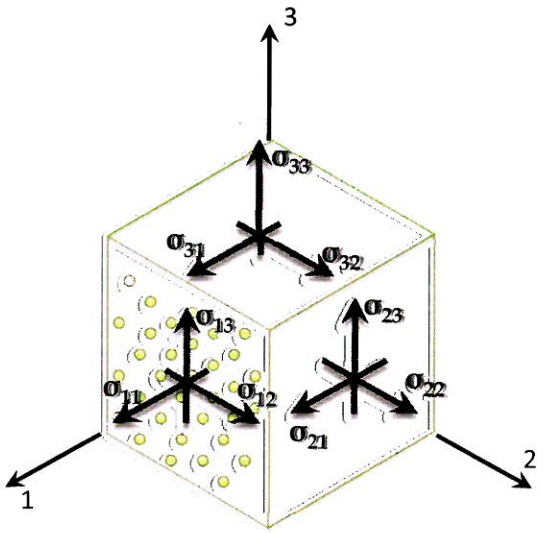

Figure 1.3: Definition of material coordinate system for UD composite ply

applications, the differently oriented lamina are stacked in a specific sequence to tailor the properties of the laminate for desired stiffness and strength required for a particular application. In this thesis, the focus is on UD composite fibre reinforced composite materials with the combination of carbon fibre and epoxy resin.

In order to distinguish the directional dependent material properties of composites, a material coordinate system (1,2,3) is introduced. Conventionally, 1-direction indicates the orientation of the reinforcing fibres, while the 2-direction is the transverse direction in the plane of the fibre reinforcement. The 3-direction usually points in the through thickness direction if the lamina is embedded in a laminate. The material coordinate system and the corresponding components of the stress tensor used within this thesis are displayed in Fig. 1.3.

Despite fundamentally known to be made of heterogeneous materials, in analysis the material properties are smeared over the volume of a Representative Volume Element (RVE) thus allowing the material to be treated as homogeneous (Herakovich, 1998). The RVE is small enough to be representative of local material response yet

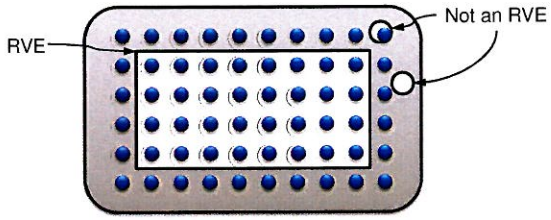

Figure 1.4: Representative Volume Element

large enough to represent 'average' material response (see Fig. 1.4). The application of homogenisation requires a strict definition of the size of a RVE for which the constitutive model is valid. The size of the RVE is dependent on the scale at which modelling is performed . The scale of the matter itself is essential to characterize failure. All failure modes have a scale of action. Composite laminates have failure modes that inherently relate to the scale of the laminate. For example, debonding of fibre/matrix interface is meaningful only at the laminate level. Kink band formation cannot be predicted from fibre scale failure. In general, three main scales are commonly identified for the composites used here (see Fig. 1.5) (Weigand, 2009). First, the microscale, where fibre, matrix and the interface between them are considered separately. Second, the mesoscale, where the lamina is considered as a homogeneous material but the interface between laminae is still considered separate. Third, the macroscale, where several laminae of different orientation are considered as one homogeneous material.

Within this thesis, the reference (initial) configuration is assumed to be stress free and the initial stresses are neglected ($\boldsymbol{\sigma^0} = \mathbf{0}$) in the generalised Hooke's law as given in Equation (1.1) assuming infinitesimal deformations

$$\begin{aligned} \boldsymbol{\sigma} &= \boldsymbol{C} : \boldsymbol{\epsilon} + \boldsymbol{\sigma^0} \\ \sigma_{ij} &= C_{ijkl}\epsilon_{kl} + \sigma^0_{ij} \end{aligned} \tag{1.1}$$

where, $\boldsymbol{C}$ denotes the fourth order tensor called elasticity tensor or stiffness tensor, with 81 elastic material parameters. Invoking symmetry of the stress tensor gives

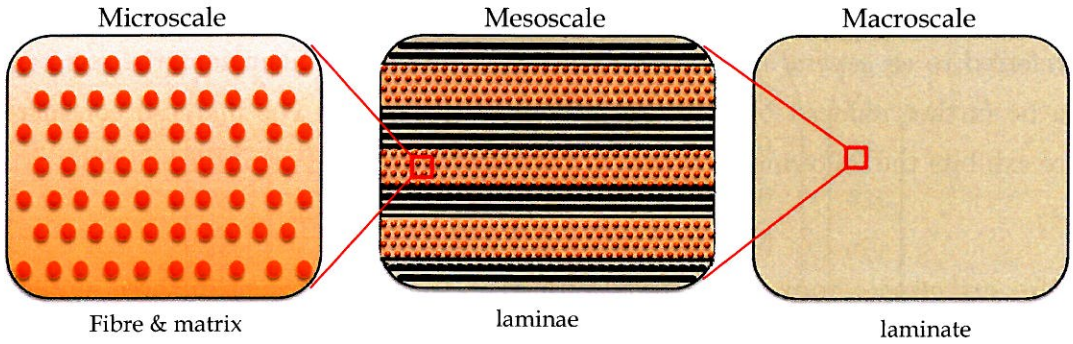

Figure 1.5: The three scales of modelling in UD composites

$C_{ijkl} = C_{jikl}$. Similarly, symmetry of the strain tensor gives $C_{ijkl} = C_{ijlk}$. Thus, the number of independent constants is reduced from 81 to 36 when the stresses and strains are symmetric.

In view of the reduced constants, Hooke's law can be written in contracted notation as

$$\sigma_i = C_{ij}\epsilon_j \quad (i, j = 1, 2, ..., 6) \tag{1.2}$$

Note that in the contracted notation $\sigma_1 = \sigma_{11}$, $\epsilon_1 = \epsilon_{11}$ and so on, and the shear strain terms are the engineering shear strains, e.g., $\epsilon_4 = 2\epsilon_{12} = \gamma_{12}$.

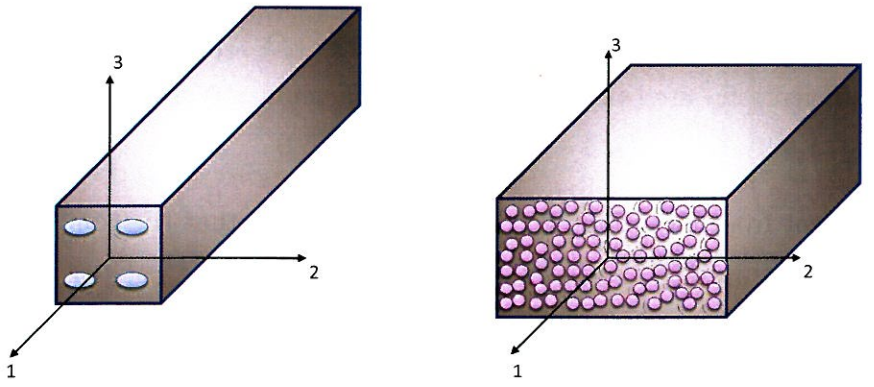

(a) Orthotropic material **(b)** Transversely Isotropic material

Figure 1.6: Material Symmetry

The symmetric stiffness matrix, C_{ij}, has 21 independent material constants. This is referred to as *general anisotropy*. The number of independent material constants can be further reduced by considering certain symmetry. The material considered here exhibits the following two cases of material symmetry (Herakovich, 1998).

An *orthotropic* body has material properties that are different in three mutually perpendicular directions at a point and, further, has three mutually perpendicular planes of material property symmetry. The planes of material symmetry are, the 1-2 plane, the 1-3 plane and the 2-3 plane (see Fig. 1.6a). As a result, the stiffness matrix has nine independent constants. Equation (1.2) then reads in matrix form as

$$\begin{pmatrix} \sigma_{11} \\ \sigma_{22} \\ \sigma_{33} \\ \sigma_{12} \\ \sigma_{23} \\ \sigma_{13} \end{pmatrix} = \begin{pmatrix} C_{11} & C_{12} & C_{13} & 0 & 0 & 0 \\ C_{12} & C_{22} & C_{23} & 0 & 0 & 0 \\ C_{13} & C_{23} & C_{33} & 0 & 0 & 0 \\ 0 & 0 & 0 & C_{44} & 0 & 0 \\ 0 & 0 & 0 & 0 & C_{55} & 0 \\ 0 & 0 & 0 & 0 & 0 & C_{66} \end{pmatrix} \begin{pmatrix} \epsilon_{11} \\ \epsilon_{22} \\ \epsilon_{33} \\ 2\epsilon_{12} \\ 2\epsilon_{23} \\ 2\epsilon_{13} \end{pmatrix} \tag{1.3}$$

The inverted form of Hooke's law (Equation (1.2)) can be written as

$$\epsilon_i = S_{ij}\sigma_j \tag{1.4}$$

where, coefficients S_{ij} are called *compliance coefficients*.

It is evident from Equation (1.2) and Equation (1.4) that the compliance matrix is the inverse of the stiffness matrix; thus,

$$S_{ij} = C_{ij}^{-1} \tag{1.5}$$

In view of the stiffness matrix being symmetric the compliance matrix is also

symmetric. Expressing Equation (1.4) in engineering notation, we have

$$\begin{pmatrix} \epsilon_{11} \\ \epsilon_{22} \\ \epsilon_{33} \\ 2\epsilon_{12} \\ 2\epsilon_{23} \\ 2\epsilon_{13} \end{pmatrix} = \begin{pmatrix} \frac{1}{E_1} & -\frac{\nu_{12}}{E_1} & -\frac{\nu_{13}}{E_1} & 0 & 0 & 0 \\ -\frac{\nu_{12}}{E_1} & \frac{1}{E_2} & -\frac{\nu_{23}}{E_2} & 0 & 0 & 0 \\ -\frac{\nu_{13}}{E_1} & -\frac{\nu_{23}}{E_2} & \frac{1}{E_3} & 0 & 0 & 0 \\ 0 & 0 & 0 & \frac{1}{G_{12}} & 0 & 0 \\ 0 & 0 & 0 & 0 & \frac{1}{G_{23}} & 0 \\ 0 & 0 & 0 & 0 & 0 & \frac{1}{G_{13}} \end{pmatrix} \begin{pmatrix} \sigma_{11} \\ \sigma_{22} \\ \sigma_{33} \\ \sigma_{12} \\ \sigma_{23} \\ \sigma_{13} \end{pmatrix} \tag{1.6}$$

From Equation (1.6) it becomes clear that the nine elastic constants for orthotropic material behavior are E_1, E_2, E_3, G_{12}, G_{23}, G_{13}, ν_{12}, ν_{23} and ν_{13}.

For some cases the UD-ply can be further simplified. A *transversally isotropic* material is defined as a material whose effective properties are isotropic in one of its planes. Assuming that the material properties are identical in any direction transverse to the fibre direction (1-direction) leads to isotropic material behavior in the 2-3 plane (see Fig. 1.6b). For symmetry about the 1-axis Equation (1.3) reduces to

$$\begin{pmatrix} \sigma_{11} \\ \sigma_{22} \\ \sigma_{33} \\ \sigma_{12} \\ \sigma_{23} \\ \sigma_{13} \end{pmatrix} = \begin{pmatrix} C_{11} & C_{12} & C_{12} & 0 & 0 & 0 \\ C_{12} & C_{22} & C_{23} & 0 & 0 & 0 \\ C_{13} & C_{23} & C_{22} & 0 & 0 & 0 \\ 0 & 0 & 0 & C_{44} & 0 & 0 \\ 0 & 0 & 0 & 0 & \frac{1}{2}(C_{22} - C_{23}) & 0 \\ 0 & 0 & 0 & 0 & 0 & C_{44} \end{pmatrix} \begin{pmatrix} \epsilon_{11} \\ \epsilon_{22} \\ \epsilon_{33} \\ 2\epsilon_{12} \\ 2\epsilon_{23} \\ 2\epsilon_{13} \end{pmatrix} \tag{1.7}$$

leaving only 5 independent material constants E_1, E_2, G_{12}, ν_{12} and ν_{23}.

Within this thesis the material is assumed to behave as orthotropic.

1.4 Failure Mechanisms

Fibre reinforced composite materials fail in a variety of mechanisms at the fibre/matrix (micro) level (see Fig. 1.7). Intralaminar failure mechanisms include *fibre fracture*, *fibre buckling* (*kinking*), *fibre splitting*, *fibre pullout*, *fibre/matrix debonding* and *matrix cracking*. At the laminate level, these failure mechanisms manifest themselves as *lamina failures* in the form of *transverse cracks* in plane parallel to the fibres, *fibre dominated failures* in plane perpendicular to the fibres, and *delaminations* between layers of the laminate.

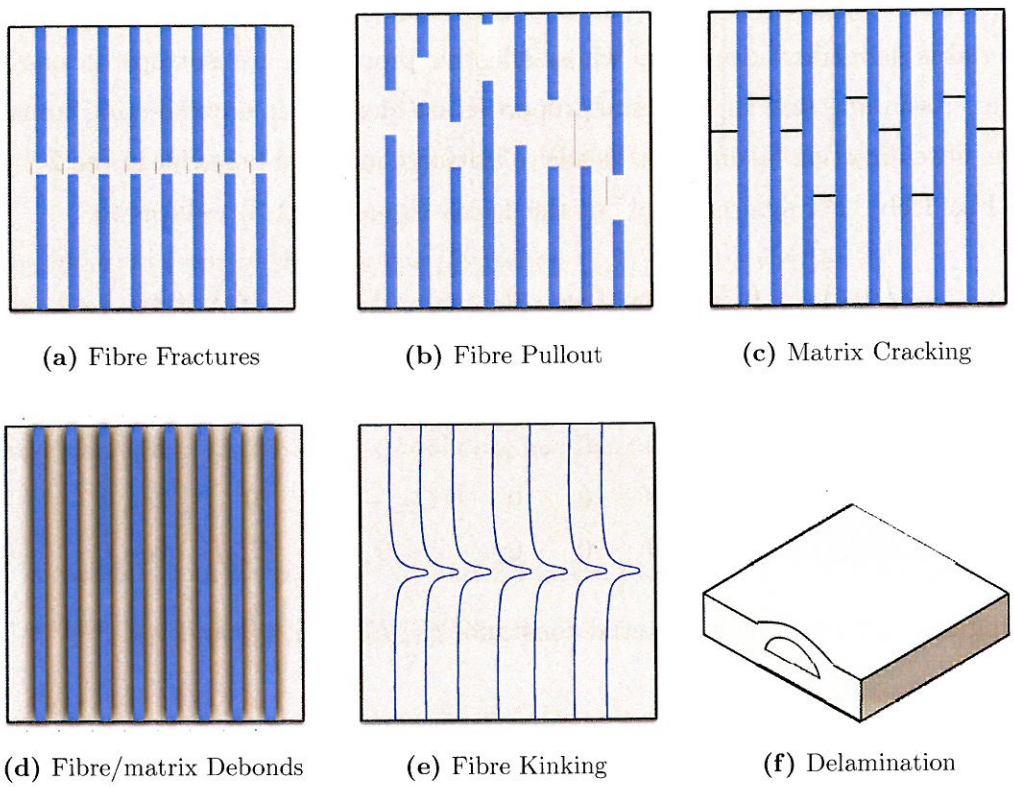

(a) Fibre Fractures **(b)** Fibre Pullout **(c)** Matrix Cracking

(d) Fibre/matrix Debonds **(e)** Fibre Kinking **(f)** Delamination

Figure 1.7: Failure Mechanisms (Herakovich, 1998)

1.5 Constitutive Modelling Framework

Fibre fracture is the most catastrophic form of failure mechanism as the fibres are typically the primary load-carrying component. Matrix cracking occurs when the strength of the matrix is exceeded. Interlaminar damage i.e., delamination is one of the predominant forms of failure in many laminated composites. It by itself may not result in catastrophic failure of the structure but can cause a significant reduction in the compressive load-carrying capacity of a structure leading to ultimate failure under the multiplication of other failure modes.

Within the framework of FE, the constitutive model has to establish the relationship between displacements and resulting nodal forces. In this thesis, the material behavior is assumed to be linear elastic initially. The characteristic rate dependent material behavior of composites, however, later results in non-linear material behavior. The constitutive model maintains the linear elastic behavior till damage is detected. After damage initiation, the strain rate dependent material behavior included in the characteristic equations results in non-linearity.

An explicit dynamic FE analysis is chosen in this thesis as it is computationally efficient for the analysis of large models with relatively short dynamic response times and for the analysis of extremely discontinuous events or processes. It also allows for the definition of very general contact conditions that can represent conditions seen in actual test cases. The non-linear problem is solved by performing a large number of small time increments efficiently. The time increment is defined by the material properties and spatial discretisation. The explicit dynamic analysis procedure is based upon the implementation of an explicit central-difference integration rule together with the use of diagonal (lumped) element mass matrices. The central-difference operator is conditionally stable and an approximation to the stability limit is often written as the smallest transit time of a dilatational wave across any of the elements

in the mesh

$$\Delta t \approx \frac{L_{min}}{c_d} \tag{1.8}$$

where, L_{min} is the smallest element dimension in the mesh and c_d is the dilatational wave speed in terms of the Lame's constants λ and μ.

In this thesis, modelling is performed on the mesoscale. The RVE here represents a single UD reinforced lamina. In the framework of FE, each finite element represents a single RVE. Consequently, the spatial discretisation of the FE model should be chosen such that the maximum permitted size of the RVE is not exceeded. A ply level discretisation is applied such that the size of the RVE is equal to only one lamina. The definition of damage initiation is formulated in terms of stress. The evolution is based on the growth of the damaged surface in stress space, which is mapped onto the corresponding surface in strain space. The strength properties provided as input, are measured values taken from literature representing an average over a certain volume.

1.6 Thesis Layout

The thesis is divided into separate chapters each dealing with a particular aspect. In the second chapter, an introduction to available composite failure theories is given with their historical progression. The focus is on novel theories within the Continuum Damage Mechanics (CDM) framework. Selected theories are briefly introduced with a mention of the detection criteria used pertaining to various damage modes. Further, insight is given into the various damage evolution models. A brief note on rate dependent behavior of composites is made.

Based on the physically based failure theories presented in Chapter 2, a composite damage model is chosen for implementation. Chapter 3 presents the details on the formulation of the chosen model into an damage evolution algorithm applied in the form of a user subroutine in **ABAQUS/Explicit** (Abaqus, 2008). The governing equations of the chosen evolution model are presented along with the flowchart of the

actual implementation in the explicit FE environment. Constitutive model verification data is presented in Chapter 4. Standard impact test(s) used in the aerospace industry are simulated and results predicted from the constitutive model are compared against published test results from literature. Based on the results, conclusions and suggestions for further research and improvement are made in Chapter 5.

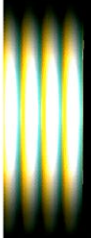

Chapter 2

Literature Survey

This chapter presents an overview of the theories that have been proposed over the years to capture the damage phenomenon observed in composite materials. Due to the scale dependence of failure modes and complications of damage, failure characterizations based on nano-scale and micro scale idealizations are not considered as established and hence not discussed. Focus is limited to physically based theories that operate on macroscopic idealizations only. Selected state-of-the-art theories are discussed in more detail.

2.1 Introduction

The strength of material used is typically established initially by prediction or test along the principal material directions. However, since practical loading in service conditions can introduce multi-axial stresses, prediction of failure taking into account arbitrary stress states is important.

Consider the case of a quasi-isotropic layup. This common form consists of equal number of plies or lamina in the 0, +45, -45 and 90 degree fiber directions. The quasi-isotropic case forms one limit of all the possible layups; the other being the unidirectional case itself. A given set of property values and application of lamina

level failure criterion results in the following sequences of some particularly important stress states as mentioned in (Christensen, 2009).

1. Uniaxial Tension
   (i) 90° matrix damage, then
   (ii) ±45° matrix damage, then
   (iii) 0° fibre failure
2. Uniaxial Compression
   (i) ±45° matrix damage, simultaneous with
   (ii) 0° fibre failure
3. Equi-Biaxial Tension
   (i) All matrix damage, then
   (ii) All fibre failure
4. Equi-Biaxial Compression
   (i) All fibre failure, no matrix damage
5. Shear (0° Tension, 90° Compression)
   (i) ±45° matrix damage, then
   (ii) 90° matrix damage, then
   (iii) 90° fibre failure

2.2 Damage Criteria

A large number of criteria predicting the behavior of composites in failure have been proposed in literature. One way to categorize them is based on how they consider the interaction between the different stress components.

(a) The simplest approaches are those where no interaction is considered i.e., strength in any one direction is not influenced by the magnitude of stresses in other directions. Typically, such criteria have one equation for each of the three in-plane stress (strain) components. Examples include the well known Maximum stress criterion and the Maximum strain criterion.
These theories have the limitation that they do not take interactions into account. This effect is accentuated in situations where transverse normal and shear stresses dominate.

(b) The interactive approaches consider the interaction between the stress components by a number of criteria. They typically suggest that the failure load in any one direction is affected by the application of loads in other directions. Typically, these criteria present a single constitutive equation to define the failure envelope. Examples of such criteria are the Tsai-Hill and the Tsai-Wu criterion. It needs to be mentioned that these criteria are derived based on linking experimental constants rather than on a physical interpretation of material behavior. The interactive criteria are often criticized for the reason that they do not take into account the failure mode in any meaningful way. The reason being it is normally expected that for the underlying physical phenomenon to be correctly represented, at least one equation is needed for each failure mode separately. The interactive criteria often use just a single equation to represent the entire failure envelope.

(c) The third approach uses criteria that are a combination of the interactive and non-interactive conditions. For example: The failure stress in the fibre direction might be taken independently of the transverse and in-plane shear stresses while the failure stresses in each of the latter might be based on an interactive condition.

The earliest efforts started with merely extending the classical strength based criteria already in use for isotropic materials to composites. This approach assumed that the linear elastic behavior of the composite is followed by a sudden lose of the

load bearing capacity. Later, the well known yield criterion for isotropic materials such as, Von-Mises and Hill, were modified and applied to define the elastic limit for a composite. The Hoffman criterion for brittle materials (Hoffman, 1967) is one such criteria which defines a single failure envelope based on stress invariants in orthotropic stress space using Hill yield criterion.The proposed criterion in principle stress space reads

$$\begin{aligned} C_1(\sigma_y - \sigma_z)^2 + C_2(\sigma_z - \sigma_x)^2 + C_3(\sigma_x - \sigma_y)^2 + \\ C_4\sigma_x + C_5\sigma_y + C_6\sigma_z + C_7\tau_{yz}^2 + C_8\tau_{zx}^2 + C_9\tau_{xz}^2 = 1 \end{aligned} \tag{2.1}$$

The nine material parameters $C_1 ... C_9$ in Equation (2.1), can be uniquely determined from the nine basic strength properties.

Tsai further developed the orthotropic yield criterion by introducing the interaction between stress terms. The Tsai-Hill criterion is an extension of the Von Mises yield criterion and is represented by the Equation (2.2)

$$\begin{aligned} (G+H)\sigma_1^2 + (F+H)\sigma_2^2 + (F+G)\sigma_3^2 - \\ 2H\sigma_1\sigma_2 - 2G\sigma_1\sigma_3 - 2F\sigma_2\sigma_3 + \\ 2L\tau_{23}^2 + 2M\tau_{13}^2 + 2N\tau_{12}^2 = 1 \end{aligned} \tag{2.2}$$

where, F, G, H, L, M and N are related to the failure strengths X, Y and S. Using appropriate relations for the various parameters, the criterion can be written in terms of the strengths as

$$\frac{\sigma_1^2}{X^2} - \frac{\sigma_1 \cdot \sigma_2}{X^2} + \frac{\sigma_2^2}{Y^2} + \frac{\tau_{12}^2}{S^2} \tag{2.3}$$

The Tsai-Wu (Tsai and Wu, 1971) criterion is defined by two strength tensors $\mathbf{F_i}$ and $\mathbf{F_{ij}}$. In tensor notation the criterion reads

$$\mathbf{F_i}\sigma_\mathbf{i} + \mathbf{F_{ij}}\sigma_\mathbf{ij} = 1 \tag{2.4}$$

The single closed failure envelope though elegant mathematically, misses the physical basis as mentioned previously. The yield criterion theories usually only predict the onset of failure but give no information regarding the present failure mode, which is crucial for damage modelling.

To have a more physical basis in the applied criteria, work on phenomologically based failure theories began in as early as 1973 with the Hashin-Rotem criterion (Hashin and Rotem, 1973). In this approach, a separate failure criteria for each failure mode was presented. The failure surface or envelope was defined separately in stress space for each failure mode. As mentioned before, the simplest physically based criteria is the maximum stress criterion where a single stress term is compared against the strength value. The Hashin -Rotem criteria for fibre failure simply read

$$\frac{\sigma_{11}}{X_t} = 1 \text{ for } \sigma_{11} > 0 \tag{2.5}$$

Adding the influence of the shear stress and assuming a linear interaction, the stress criteria can be combined in the following form

$$\frac{\sigma_{11}}{X_t} + \left|\frac{\sigma_{12}}{S_{12}}\right| = 1 \tag{2.6}$$

An extended theory was proposed by Hashin (Hashin, 1980) later which considered a higher order of interaction between the stress terms.

$$\left(\frac{\sigma_{11}}{X_t}\right)^2 + \left(\frac{\sigma_{12}}{S_{12}}\right)^2 = 1 \tag{2.7}$$

The quadratic order of interaction is seen to fit very well with the experimental data and hence, is used very commonly in many failure mode based criteria.
A schematic comparison of the failure envelope as defined by the failure criteria example above is presented in Fig. 2.1.

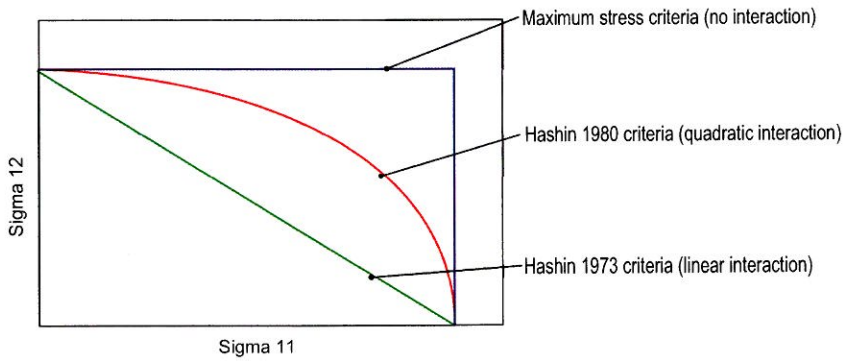

Figure 2.1: Influence of the order of interaction on the predicted failure envelope

In the subsequent years, a large number of failure theories based on both tensor polynomial criteria and failure mode criteria, have been proposed. Two distinct concerns had been emerging out of this development.

1. There did not seem a universal definition of *failure* for the composites. It was defined and understood depending on the application.

2. There was no single theory which was accepted as a universal theory to give meaningful and accurate prediction of damage phenomenon in composite structures. Even at a lamina and laminate level, there was lack of faith in the current theories.

An attempt to alleviate these concerns was undertaken in the *World Wide Failure Exercise(WWFE)* initiated by Hinton and Soden (Hinton and Soden, 1998). The objective was to put up an exercise, which would help verify the validity of various theories in use by subjecting them to predict failure in a variety of carefully chosen test cases, which could challenge the theories to maximum extent in various directions and expose their limitations and/or their adaptability and robustness. Initially, the exercise was done in two parts: in part A (Kaddour et al., 2004a), predictions were invited from participants for certain laminate configurations and material properties, purely based on their theory without having any knowledge of the experimental results. After the strength predictions were submitted, the participants were given the

experimental test results for each of the test cases and allowed to refine their theories for better correlation with the test data in part B (Kaddour et al., 2004b) of the exercise. A comparative analysis result of the theories with the test data was obtained. The results of the exercise were summed up after elaborate data analysis. Additional theories were considered and a final ranking was given in 2004 (Kaddour et al., 2004c). Overall, the following conclusions were drawn from the analysis:

- Each of the theory generated a unique biaxial failure envelope for the test types considered and some theories even predicted uniaxial strength data different to those measured and provided as input data.

- The ambiguity in accounting for thermal stresses resulted in varying and completely different failure load predictions.

- The methods used to predict laminate behavior after initial failure differed from each other and some participants gave particularly low value for the final failure.

- Even for the most familiar cases, the failure strengths predicted by the participating theories varied by huge margins.

Out of the 19 participating theories, 5 were selected to be the most promising. The leading theories were proposed by Tsai (Liu and Tsai, 1998), Puck (Puck and Schurmann, 2002), Cuntze (Cuntze and Freund, 2004), Bogetti (Bogetti et al., 2004) and Zinoviev (Zinoviev et al., 1998). Of the 5 best, only Tsai's theory was of tensor polynomial nature. It was generally agreed that physically based failure theories gave qualitatively better results.

Since the focus of this thesis is to work with a physically based failure theory, available failure criteria of some selected physically based theories are discussed in more detail in the following section influenced heavily by the work presented in (Weigand, 2009).

2.3 Damage Initiation Methodologies

2.3.1 Fibre Failure Prediction

The failure of the reinforcing fibers could be tensile or compressive in nature. The tensile failure of the fibers is commonly referred to as *Fibre rupture*. As mentioned in Section 2.1, fibre damage is usually the last mode of failure and indicates the complete failure of the lamina. Since 1969, the maximum stress criterion has been used for the fibre failure. This gives acceptable results in the tensile load regime.

For a shear stress regime, the criterion was simply written as

$$\frac{\epsilon_1}{\epsilon_{1T}} = 1 \quad \text{for} \quad \epsilon_1 > 0 \quad \text{or} \quad \frac{\epsilon_1}{\epsilon_{1C}} = -1 \quad \text{for} \quad \epsilon_1 < 0 \tag{2.8}$$

However, Equation (2.6) and Equation (2.8) do not consider the influence of other components of stress.

Puck and Schuermann (Puck and Schurmann, 2002) proposed a hypothesis that the fibre failure in a UD composite under influence of other components of stresses occurs at the same fibre stress as under a uniaxial σ_1 state of stress. This resulted in the following criteria for tensile failure:

$$\frac{1}{\epsilon_{1T}}(\epsilon_1 + \frac{\upsilon_{f12}}{E_{f1}} m_{\sigma f} \cdot \sigma_2) = 1 \quad \text{for} \quad (\ldots) > 0 \tag{2.9}$$

For a plane state of stress $(\sigma_1, \sigma_2, \tau_{12})$, the strain ϵ_1 and ϵ_{1T} are given from the expressions

$$\begin{aligned} \epsilon_1 &= \frac{\sigma_1}{E_1} - \frac{\upsilon_{12}}{E_1}\sigma_2 \\ \epsilon_{1T} &= \frac{X_T}{E_1} \end{aligned} \tag{2.10}$$

The above strain definitions when replaced in Equation (2.9) result in the criteria

$$\frac{\sigma_1}{X_T} - \upsilon_{12}\frac{\sigma_2}{X_T} + \upsilon_{f12}\frac{E_1}{E_{f1}}m_{\sigma f}\frac{\sigma_2}{X_T} = 1 \tag{2.11}$$

It was seen that the above more "physically correct" formulation did not yield a significantly improved or different result from the maximum stress criterion. A very commonly used criterion nowadays is the one proposed by Hashin (Hashin, 1980) which involves a quadratic interaction between the normal stress σ_{11} in the fibre direction and the two shear stresses σ_{12} and σ_{13} normal to the fibre direction.

$$\left(\frac{\sigma_{11}}{X_T}\right)^2 + \left(\frac{\sigma_{12}}{S_{12}}\right)^2 + \left(\frac{\sigma_{13}}{S_{13}}\right)^2 = 1 \tag{2.12}$$

The compressive failure of fibers is not so simple and is understood to occur by various different modes. For this reason, this topic has been a particular area of interest for researchers. The various failure modes of the fiber in compression have been categorized by Fleck (Fleck, 1997) into:

- *Elastic micro-buckling*
- *Plastic micro-buckling*
- *Fibre crushing*
- *Splitting*
- *Buckle delamination*
- *Shear-band formation*

The first theories concerning compressive fibre failure were proposed by Rosen (Rosen, 1965) who postulated elastic instability to be the cause of failure. Through his work, he was able to show that for a UD composite with 30% or more fibre volume fraction, as is commonly found in many applications, the material would fail in shear mode at a compressive stress

$$\sigma_c = \frac{G}{1 - \upsilon_f} \tag{2.13}$$

where, G denotes the shear modulus of the matrix and υ_f the fibre volume fraction. However, the comparisons with experimental results showed that the predicted compressive strength was too high.

The theory was further extended by Argon (Argon, 1972) who considered the perfect plastic behavior of the matrix and an initial fibre misalignment $\phi°$. It was postulated that the matrix deforms inelastically and fails to support the fibers, which start to rotate. As this rotation increases the fibers finally break to form a kink band, giving raise to the name *Fibre kinking* or *Plastic micro-buckling.* The critical failure stress is given by

$$\sigma_c = \frac{Y_c}{\phi°} \tag{2.14}$$

where, Y_c denotes the yield stress of the matrix.

This theory was further extended by Budiansky (Budiansky, 1983) by adding the shear strain term to the failure stress

$$\sigma_c = \frac{Y_c}{\gamma_c + \phi°} \tag{2.15}$$

where, γ_c is the shear strain at yield.

Experimental studies have supported the theory by Argon with the initial fibre misalignment in a carbon/PEEK composite measured as $\phi° = 3°$.

Davila and Camanho (Davila et al., 2005) and Pinho (Pinho, 2005) extended the initial kinking theory, which assumes an initial fibre misalignment for a plane state of stress. As per Davila (Davila et al., 2005), the total fibre misalignment at failure ϕ^c is composed of the initial fibre misalignment ϕ° and an additional misalignment ϕ^e caused by elastic deformation as load is applied

$$\phi^c = \phi^\circ + \phi^e \tag{2.16}$$

The theory was further extended to 3D by Pinho et al. (Pinho et al., 2006b). Instead of a single kink band, three different angles, the kink band angle ψ, the misalignment angle ϕ and the orientation of the matrix fracture plane θ were defined to express the orientation of the kink band.

The *Fibre crushing* type of fibre failure in composites occurs when the fibre crushing strength is lower than the matrix yield strength. This type of failure is not seen in modern carbon fibre/epoxy composites except for those used in low temperature applications.

Buckle delamination type of compressive failure is important for damage tolerant structures. Under subsequent compression after impact case, the delamination generated due to manufacturing problems or low velocity impact (LVI) grows and can cause failure of adjacent fibers due to buckling.

Failure modes of *Splitting* and *Shear-band formation* are mainly related to ceramic matrix composites or composites with very low fibre volume fractions.

2.3.2 Matrix Failure Prediction

The topic of matrix failure in composites is broadly referred to as the Inter Fibre Failure (IFF). This is appropriate since apart from Fibre failure (FF), the other type of failure could be either fracture of the matrix itself or the fracture of the fibre-matrix

interface. It is experimentally observed that IFF is of brittle nature.

An initial effort on the prediction on IFF modes was presented by Hashin (Hashin, 1980). This was based on the idea by Mohr who postulated that failure is caused by only those stresses which act on the fracture plane. The proposed criteria by Hashin for IFF and a plane state of stress read

$$\begin{aligned} \left(\frac{\sigma_{22}}{Y_t}\right)^2 + \left(\frac{\sigma_{12}}{S_{12}}\right)^2 &= 1 \quad \text{for} \quad \sigma_{22} \geq 0 \\ \left(\frac{\sigma_{22}}{2S_t}\right)^2 + \left(\left(\frac{Y_c}{2S_t}\right) - 1\right)\frac{\sigma_{22}}{Y_c} + \left(\frac{\sigma_{12}}{S_{12}}\right)^2 &= 1 \quad \text{for} \quad \sigma_{22} \leq 0 \end{aligned} \tag{2.17}$$

where S_t is an out of plane shear strength (S_{23} or S_{13}).

Though Hashin proposed a three dimensional failure criterion based on the suggestion of failure planes as proposed by Mohr, the idea was not pursued due to the computational effort required in finding a plane with the critical orientation resulting in IFF. This idea of the critical fracture plane however, has been used in principle by many investigators. Very recently Weigand (Weigand, 2009) as part of his doctoral studies has proposed a Golden search algorithm to efficiently determine the critical angle.

Puck (Puck and Schurmann, 2002) proposed his model based on the above mentioned idea of the fracture plane. The fracture plane for IFF is assumed to be a plane parallel to the fiber directions. This plane is inclined from the 3-axis by an angle θ. The failure criterion is written in terms of the stresses acting on the fracture plane.

$$\begin{aligned} \left(\frac{\sigma_n}{R_n^{(+)}}\right)^2 + \left(\frac{\tau_{n1}}{R_{n1} - p_{n1}\sigma_n}\right)^2 + \left(\frac{\tau_{nt}}{S_{nt} - p_{nt}\sigma_n}\right)^2 &\geq 1 \quad \text{for} \quad \sigma_n \geq 0 \\ \left(\frac{\tau_{n1}}{R_{n1} - p_{n1}\sigma_n}\right)^2 + \left(\frac{\tau_{nt}}{S_{nt} - p_{nt}\sigma_n}\right)^2 &\geq 1 \quad \text{for} \quad \sigma_n < 0 \end{aligned} \tag{2.18}$$

where, σ_n is the normal traction and τ_{n1} and τ_{nt} are the shear tractions acting on the

fracture plane.

The increase of shear strength under compressive normal stress on the fracture plane is represented by the slope parameters p_{n1} and p_{nt}. R_{n1} and R_{nt} characterize the resistance of the fracture plane against shear failure while $R_n^{(+)}$ is the resistance against tensile failure on the fracture plane.

In parallel with Puck, Cuntze and Fruend (Cuntze and Freund, 2004) developed the failure mode concept. Cuntze defined his failure criteria in terms of stress invariants instead of fracture plane and hence, avoided the expensive computational effort to determine the critical fracture plane angle. The failure surface consists of three different failure criteria, each characterizing a particular failure mechanism and incorporating one strength parameter only. The first IFF mode is a tensile failure transverse to the fibre, characterized by the transverse tensile strength Y_t. The second IFF mode is a shear failure resulting in a matrix crack oriented at $\theta_{fr} = 0°$ and is characterized by the in-plane shear strength S_{12}. The third IFF mode results in a fracture plane inclined by $\theta_{fr} \neq 0°$ and is characterized by transverse compressive strength Y_c.

$$\begin{aligned} IFF1: \; & F_{\perp}^{\sigma} = \frac{I_2 + \sqrt{I_4}}{2Y_t} = 1 \\ IFF2: \; & F_{\perp\parallel} = \frac{I_3^{2/3}}{S_{12}^3} + b_{\perp\parallel}\frac{I_2 I_3 - I_5}{S_{12}^3} = 1 \\ IFF3: \; & F_{\perp}^{\tau} = (b_{\perp}^{\tau} - 1)\frac{I_2}{Y_c} + \frac{(b_{\perp}^{\tau} - 1)I_4 + b_{\perp\parallel}^{\tau} I_3}{Y_c^2} = 1 \end{aligned} \tag{2.19}$$

where, parameter b characterizes the slope of the failure envelopes and I denotes the five stress invariants chosen to best describe the multi-axial behavior of the material. In addition, Cuntze defined mixed failure domains where certain failure modes interact and a power law was used to characterize the interaction in these zones to obtain the final failure locus.

2.3.3 Delamination Failure Prediction

Delamination is one of the most common and widely observed type of failure in laminated composites. Pagano and Schoeppner (Pagano and Schoeppner, 2000) categorize the technological causes of delamination in two categories; the first category includes delamination due to curved sections, such as tubular sections, curved segments, cylinders and spheres. In all these cases, the normal and shear stresses at the interface of plies can lead to loss of adhesion and initiation of inter laminar crack. The second category includes abrupt changes of sections such ply drop-offs, free edges and bonded and bolted joints.

An additional category can be related to temperature and moisture effects. The delaminations in this case are attributed to the differential rate of contraction between the matrix and reinforcement during the curing process (Tay and Shen, 2002). Similarly, difference in the rate of absorption of moisture by the plies may also serve as a source of this failure mode (Kim and Crasto, 1994). The manufacturing stage also can induce delaminations from poor practices of laying the plies.

According to Bolotin (Bolotin, 1996, 2001), delaminations can be considered to be of two types: internal delaminations and near-surface delaminations. Internal delaminations originate due to the interaction of matrix cracks and ply interfaces in the inner ply interfaces. This type of delamination considerably reduces the load-capacity of the composite structure particularly when compressive loads are applied. Delaminations originated by transverse matrix cracks orthogonal to tensile loads is a common example. Near-surface delaminations represent a more complex scenario than internal delaminations. Since they originate near the surface, they are less influenced by the deformation of the laminate. Hence, not only their growth but also the local stability is a matter of importance.

Irrespective of the type of delamination, this damage mode is particularly important for the structural integrity of the laminate as it is difficult to detect but causes

a reduction in the strength. Damage initiation criteria for delamination mode of failure fall under two different types of approaches; one a direct application of Fracture Mechanics and the other a formulation within the framework of Damage mechanics.

In the Fracture Mechanics approach, strain energy rate is computed and delamination growth is predicted when a combination of the components of the energy release rate G is equal to, or greater than, a critical value G_c. A simple example of this approach as proposed by O'Brien reads

$$G = \frac{t\epsilon_{11}^2}{2}(E_1^0 - E_1^{dam}) \tag{2.20}$$

where, G is the strain energy per unit of delaminated area, E_1^0 refers to the original longitudinal laminate Young's modulus and E_1^{dam} refers to the longitudinal Young's modulus of the remaining sub-laminates after delamination. In Equation (2.20), t refers to the thickness of the laminate.

A very widely used procedure to predict crack propagation is the Virtual Crack Closure Technique (VCCT) (Hallett et al., 2008). This technique is based on Irwin's assumption that when a crack extends by a small amount, the energy released in the process is equal to the work required to close the crack to its original length. The mode I, mode II and mode III energy release rates, G_I, G_{II} and G_{III} respectively can be computed from the nodal forces and displacement obtained from the solution of a finite element model. The total energy release rate reads

$$G_T = G_I + G_{II} + G_{III}$$

Crack propagation is predicted when G_T equals or exceeds G_c.

The VCCT technique is based on the assumption of self-similar propagation and hence, crack initiation and short cracks cannot be predicted. An initial delamination must be defined and for certain geometries and load cases, the location of the delam-

ination front might be difficult to predict a-priori. The good thing is that it is based on energy rather than stress.

Various different sophisticated methods of computation of strain energy release rates have been proposed, however they might require nodal variables and topological information from the nodes ahead and before the crack front and as such pose difficulties for a progressively advancing crack. Since, Fracture Mechanics technique cannot be applied without an initial crack definition, they are more suitable for application in damage propagation more than damage initiation.

In Damage Mechanics approach, an early failure criteria based on stress was proposed by Whitney et al. (Whitney and Nuismer, 1974). The idea of a dimension parameter, which defined the distance from a stress concentration over which the material must be critically stressed in order to initiate failure was defined. This idea was applied to delamination failure by Brewer (Brewer and Lagace, 1988) who formulated his criterion based on average stress. The parameter x_{avg} which is an experimentally obtained averaging dimension was used to average localized stresses as

$$\overline{\sigma}_{ij} = \frac{1}{x_{avg}} \int_0^{x_{avg}} \sigma_{ij} dx \tag{2.21}$$

where, x is the distance from the free edge. The averaged stresses are then used in the following interaction criteria

$$\frac{\overline{\sigma}_{13}{}^2}{S_{13}} + \frac{\overline{\sigma}_{23}{}^2}{S_{23}} + \frac{\overline{\sigma}^t_{33}{}^2}{Z_{tt}} + \frac{\overline{\sigma}^c_{33}{}^2}{Z_c} = 1 \tag{2.22}$$

In Equation (2.22), the contribution of compressive stresses normal to the delamination plane is taken towards onset of delamination. This is counter intuitive at first as it is widely believed that compressive stresses impede the growth of delamination. However, Hou and Petrinic (Hou et al., 2001) suggest through their studies that under a certain limit of normal compressive stresses delaminations can still develop. They suggest that only when the normal compressive stresses have grown to be at least

twice as large as the sum of the transverse shear stresses, the delamination growth is impeded. The modified criteria for delamination is thus given by them as

$$\begin{aligned} \left(\frac{\sigma_{33}}{Z_t}\right)^2 + \left(\frac{\sigma_{13}+\sigma_{23}}{S_d}\right)^2 &= 1 \text{ for } \sigma_{33} \geq 0 \\ \left(\frac{\sigma_{13}+\sigma_{23}}{S_d}\right)^2 - 8\left(\frac{\sigma_{33}}{S_d}\right)^2 &= 1 \text{ for } -\sqrt{\frac{(\sigma_{13}^2+\sigma_{23}^2)}{8}} \leq \sigma_{33} < 0 \end{aligned} \tag{2.23}$$

where, Z_t is the through thickness tensile strength and S_d is the out of plane shear strength.

Another stress based criteria for delamination is the application of IFF model of Puck (Puck and Schurmann, 2002) transverse to the fibre direction in a UD lamina. Delamination is treated as a matrix crack with a fracture angle of $\theta_{fp} = 90°$. However, with this model it was reported (Weigand, 2009) that they are valid only within a UD lamina. For neighboring plies with a different fibre orientation, the Puck criterion is not able to predict delamination.

Another concept is the use of cohesive crack model: a cohesive damage zone is developed near the crack front. The origin of the cohesive crack model goes back to Dugdale (Dugdale, 1960) who introduced the concept that stresses in the material are limited by the yield stress and a thin plastic zone is generated in front of the notch.

Cohesive damage zone models (Pinho et al., 2006a; Turon et al., 2006; Camanho et al., 2003) relate tractions to displacement jumps at an interface where a crack may occur. Damage initiation is related to the inter-facial strength, i.e., the maximum traction τ° in the traction-displacement jump relation. When the area under the traction-displacement jump relation is equal to the fracture toughness G_c, the traction is reduced to zero and new crack surfaces are formed. For an undamaged interface, delamination starts when a scalar function of the inter-laminar stresses reaches a limit.

The damage initiation is represented as

$$f(\tau_i) = 1 \tag{2.24}$$

where, $f(\tau_i)$ is a norm of the tractions.

(Camanho et al., 2003) developed zero thickness volumetric decohesion elements that use a quadratic interaction between tractions for the prediction of delamination propagation. The constitutive law for the damage onset was predicted using the criteria as given in Equation (2.25)

$$\left(\frac{\langle \tau_3 \rangle}{N}\right)^2 + \left(\frac{\tau_2}{S}\right)^2 + \left(\frac{\tau_1}{T}\right)^2 = 1 \tag{2.25}$$

where, N, S, and T represent the strengths in the corresponding directions of the tractions τ.

(Turon et al., 2006) proposed similar damage model which was thermodynamically consistent and accounts for the changes in the loading mode. It also accounts for crack closure effects to avoid interfacial penetration of two adjacent layers after complete decohesion. This model was based on the framework of damage mechanics with the constitutive equation for the interface derived from the free energy of the interface. A single scalar variable was proposed to track damage at the interface under general loading conditions.

Models based on Ye's criterion (Ye, 1988) use a quadratic interaction of the tractions to represent a mixed mode of failure

$$\left(\frac{\langle \tau_3 \rangle}{\tau_3^\circ}\right)^2 + \left(\frac{\tau_2}{\tau_2^\circ}\right)^2 + \left(\frac{\tau_1}{\tau_1^\circ}\right)^2 = 1 \tag{2.26}$$

where, $\langle \cdot \rangle$ is the McAuley bracket defined as $\langle x \rangle = \frac{1}{2}(x + |x|)$.

2.4 Damage Evolution Methodologies

During the loading of various lamina within a laminate, both matrix controlled and fibre controlled types of failure can separately and sequentially occur. At some point so much damage has accumulated in the form of these local failures that the laminate can no longer sustain any load. This then, comprises the ultimate load, failure in the broad and total sense.

A careful accounting and sequencing of failure after an initial criteria is met is required to predict complete failure of composites. The complex failure behavior and simultaneous occurrence of several failure modes has ensured that damage evolution has been a constant focus of research in the composite community. A brief overview of the damage evolution concepts as applied are presented in the following sections.

2.4.1 Continuum Damage Mechanics models for Intra-laminar Failure

Weigand (Weigand, 2009) cites that an early work in the representation of damage in the continuum damage model by an internal damage variable applied to failure modelling of creep rupture is attributed to Kachanov. This approach was further developed and the parameter $(1 - \omega)$ was introduced as a measure of the damage due to void growth and coalescence. The parameter ω is defined as change of cross-sectional area as a consequence of void growth i.e.,

$$\hat{A} = A(1 - \omega) \tag{2.27}$$

where, $\hat{A}$ is the effective area and A is the original undamaged area.

In order to introduce the directional dependence, a damage tensor was proposed and the relation between the damage tensor and elastic constants was established by Lemaitre and Chaboche (Lemaitre and Chaboche, 1978).

Most of the Continuum Damage Mechanics (CDM) models rely on representation of damage by introducing a set of internal damage variables or damage tensor as mentioned above. The differences arise in the definition of damage evolution. One of the simplest models, the well known Chang-Chang model (Chang and Chang, 1987), which is implemented into the commercial FE solver LS-DYNA, uses a damage evolution rule where the damage variable is a function of the step time. The elastic properties are diminished within 100 time steps as soon as damage initiation is predicted. There is no dependence on the load or deformation and hence, this model is not very realistic.

Another model which is based on the use of thermodynamic potentials was proposed by Ladeveze and Le Dantec (Ladeveze and LeDantec, 1992) and Matzenmiller (Matzenmiller et al., 1995). Internal variables which characterize damage are introduced into strain energy function

$$U = \mathrm{f}(\sigma, \omega) \tag{2.28}$$

The energy release rate per unit volume $\mathbf{Y}$ is then given by

$$Y_i = \frac{\partial U}{\partial \omega_i} \tag{2.29}$$

$\mathbf{Y}$ characterizes energy release or dissipation due to increasing damage. They govern damage development, just as energy-release rate governs crack propagation. Based on these energy release rates $\mathbf{Y}$(also referred to as conjugated forces or thermodynamic forces), damage evolution laws can be defined. Usually, one thermodynamic force is associated with one damage internal variable.

The Ladeveze model (Ladeveze and LeDantec, 1992), implemented in commercial FE solver PAMCRASH, proposed simple damage evolution laws where damage

variable ω is defined as a function of $\mathbf{Y}$

$$\omega_i = \frac{\langle Y_i - Y_o \rangle}{Y_c} \tag{2.30}$$

where, Y_o and Y_c are threshold values which control the onset of damage evolution for the respective damage mode. $\langle \cdot \rangle$ is the McAuley bracket defined as $\langle x \rangle = \frac{1}{2}(x + |x|)$ Y_i is the maximum value over the loading history defined as

$$Y_i(t) = \max(\sqrt{Y_i(\tau)}) \quad \text{with } \tau \geq t \tag{2.31}$$

where,

$$\begin{aligned} Y_{1,2}(\tau) &= \frac{1}{2}\left(\frac{\sigma_{1,2}^2}{E_{1,2}(1-\omega_{1,2})^2}\right) \\ Y_{12}(\tau) &= \frac{1}{2}\left(\frac{\sigma_{12}^2}{G_{12}(1-\omega_{12})^2}\right) \end{aligned} \tag{2.32}$$

It is to be noted that this model was based on a plane-stress state assumption and the damage variables were denoted by the letter d. Here, ω is used to maintain consistency within the document.

The Matzenmiller model (Matzenmiller et al., 1995) defined a strain rate dependent damage evolution law, which is driven by scalar growth functions ϕ_i and vector functions $\mathbf{q}_i$. The rate of damage evolution is given by

$$\dot{\boldsymbol{\omega}} = \sum_i \phi_i \, \mathbf{q}_i \tag{2.33}$$

The growth function ϕ_i is a function of the strain rate and damage state and is derived from strain based failure criteria, which in turn is derived from stress based failure criteria. The vector functions $\mathbf{q}_i$ are also referred to as damage directors and provide information about the coupling of different damage mechanisms. This model is discussed in detail in Section 3.3. Recently, Curiel Sosa (Curiel et al., 2008) ex-

tended the Matzenmiller model defined for plane stress into three dimensional stress states.

Maimí (Maimí et al., 2007a,b) proposed another CDM model for plane stress based on concept similar to that of Matzenmiller. Physical based failure criteria are used to define a set of loading functions in stress space and their gradient is used to evaluate the onset and evolution of damage. Elastic domain threshold variables r_i are introduced into the failure criteria to represent the shrinking elastic domain for increasing damage. In case of predicted damage evolution the rate of shrinkage of elastic domain $\dot{r}_i$ is obtained from the loading function gradient. The damage variables are then defined as a function of g_i and energy dissipation due to crack growth. Damage evolution is then driven by the rate at which the failure surface is exceeded. The model takes into account the orientation of the fracture plane for compressive IFF, however the fracture plane orientation is set to a constant angle and not calculated explicitly.

A three dimensional CDM model was proposed by Pinho (Pinho et al., 2006b,c) recently. The model relies on the approach of using fracture energy as a driving parameter for damage evolution. The rate of damage growth per increment of deformation is calculated such that the dissipated energy corresponds to experimentally obtained fracture energies. Hence, the energy release rates are fit to experimental data rather than calculated from thermodynamic potentials.

2.4.2 Delamination Propagation

For Delamination failure mode, which is an inter-laminar kind of failure and appears on a macro scale, both fracture mechanics and damage mechanics formulations have been used to describe propagation. Recent review by Elder (Elder et al., 2004) compares both the approaches for delamination propagation under low velocity impact.

Damage mechanics approach is used when the interface region is modelled as a resin rich zone between the plies. These models use the CDM approach using damage

variables to track the damage growth. In this approach, the actual crack between the plies cannot be simulated for obvious reasons, however the regions of delamination presence can be effectively predicted. It should be mentioned that with an element deletion feature, it is still possible to simulate a crack opening like scenario.

Fracture mechanics approach is a more appropriate option for this mode of failure due to its very nature. With recent formulations involving cohesive zone modelling, more realistically appearing simulations have appeared. The interface is modelled as system of springs which connect the nodes of adjacent plies. Damage laws are introduced which relate the force or regularized stress between nodes to opening displacement δ. Once the critical opening is reached the springs are removed, thus simulating a crack opening. In order to correctly represent the release of energy due to crack propagation, the critical opening displacement is often chosen such that the released energy corresponds to the fracture energy of the material.

Following the initiation criteria as shown in Equation (2.24), the propagation criteria can be represented as

$$\mathrm{f}(G_i) = 1 \tag{2.34}$$

where, $\mathrm{f}(G_i)$ is a norm of the energy release rates. Using the power law criteria for mixed mode situation, the expression becomes

$$\left(\frac{G_I}{G_{I_c}}\right)^{\alpha} + \left(\frac{G_{II}}{G_{II_c}}\right)^{\beta} + \left(\frac{G_{III}}{G_{III_c}}\right)^{\gamma} = 1 \tag{2.35}$$

where, G_I, G_{II} and G_{III} are the individual components of the energy release rates in mode I, mode II and mode III respectively. The parameters α, β and γ are chosen to fit experimental data. Frequently, $\alpha = \beta = \gamma = 1$ (linear) or $\alpha = \beta = \gamma = 2$ (quadratic) is chosen.

Cohesive zone models using decohesive elements to predict delamination propagation use a softening law with a single relative displacement damage parameter to track

the damage state of the interface. Camanho (Camanho et al., 2003) also show that the expression proposed by (Benzeggagh and Kenane, 1996) for the critical energy release rate for a mixed-mode ratio is more accurate for epoxy and PEEK composites. The softening law of Benzeggagh-Kenane is represented as

$$G_c = G_{Ic} + (G_{IIc} - G_{Ic} \left(\frac{G_{shear}}{G_T} \right)^{\eta} \tag{2.36}$$

Delamination growth is produced when the total energy release rate G is greater or equal than the critical value G_c. The energy release rate under mixed-mode loading is $G = G_I + G_{shear}$, where $G_{shear} = G_{II} + G_{III}$ is the energy release rate for shear loading.

2.5 Influence of Rate Dependency

Composite materials demonstrate a very pronounced effect of the strain rate on the material behavior. The mechanical properties not only change with the direction in which loading is applied but also with the rate at which load is applied. This is attributed to the viscoelastic behavior of the matrix material. In highly dynamic situations such as impact problems, this effect is very pronounced.

Weigand (Weigand, 2009) provides a detailed review and experimental study on this topic and refers to the work by (Cantwell and Morton, 1991) who provides a review of the major tendencies and results in this area. The conclusions are drawn based on experimental observations from tests conducted on carefully chosen specimens. A big chunk of the data is generated from large scale experiments such as impact experiments, which however result in complex stress states making it difficult to establish the rate dependency clearly. Rate dependency, however, is well accessed from controlled experiments involving simpler stress states such as uniaxial tests.

Very few experimental data is available for strain rate dependence attributed to

epoxy resins. It has been reported from the study carried out at University of Oxford (Heigand, 2009) that an initial linear change of properties switches to an exponential increase at certain strain rate, which is different for each epoxy.

The behavior of carbon fibre reinforced polymers under tensile loading in fibre direction is widely regarded to be rate insensitive, however the failure in compression is dependent on the strain rate. The reason is that failure in compression is highly governed by the behavior of the matrix and interface between fibre and matrix.

The data on rate dependent behavior transverse to the fibre direction can be divided into two groups. While one group indicates significant strain rate effects, the other suggests non or only mild rate dependent behavior. It is suggested that such a difference arises due to the strong dependency of the results on the testing method or specimen geometry. The behavior is largely believed to be similar to epoxy resin behavior mentioned previously. Both the tensile and compressive material properties seem to follow this trend the best.

The available data on out of plane shear suggests that it is not governed by the strain rate. This is quite surprising as the failure mode associated with inter-laminar shear stress between plies i.e., delamination, is basically a failure of the matrix in the interface between the plies, which is understood to be rate dependent.

2.6 Summary

In this chapter, a brief historical overview on the various failure theories for unidirectional composites was presented. The initial part dealt with the initiation criteria for the failure modes of fibre failure, matrix failure and delamination as has been reported in literature. Specific contributions to fibre kinking brought the application of a kink plane to define the damage criteria into focus. This has been in contrast of applying failure criteria to damage planes for the other

the damage state of the interface. Camanho (Camanho et al., 2003) also show that the expression proposed by (Benzeggagh and Kenane, 1996) for the critical energy release rate for a mixed-mode ratio is more accurate for epoxy and PEEK composites. The softening law of Benzeggagh-Kenane is represented as

$$G_c = G_{Ic} + (G_{IIc} - G_{Ic} \left(\frac{G_{shear}}{G_T} \right)^{\eta} \tag{2.36}$$

Delamination growth is produced when the total energy release rate G is greater or equal than the critical value G_c. The energy release rate under mixed-mode loading is $G = G_I + G_{shear}$, where $G_{shear} = G_{II} + G_{III}$ is the energy release rate for shear loading.

2.5 Influence of Rate Dependency

Composite materials demonstrate a very pronounced effect of the strain rate on the material behavior. The mechanical properties not only change with the direction in which loading is applied but also with the rate at which load is applied. This is attributed to the viscoelastic behavior of the matrix material. In highly dynamic situations such as impact problems, this effect is very pronounced.

Weigand (Weigand, 2009) provides a detailed review and experimental study on this topic and refers to the work by (Cantwell and Morton, 1991) who provides a review of the major tendencies and results in this area. The conclusions are drawn based on experimental observations from tests conducted on carefully chosen specimens. A big chunk of the data is generated from large scale experiments such as impact experiments, which however result in complex stress states making it difficult to establish the rate dependency clearly. Rate dependency, however, is well accessed from controlled experiments involving simpler stress states such as uniaxial tests.

Very few experimental data is available for strain rate dependence attributed to

epoxy resins. It has been reported from the study carried out at University of Oxford (Weigand, 2009) that an initial linear change of properties switches to an exponential increase at certain strain rate, which is different for each epoxy.

The behavior of carbon fibre reinforced polymers under tensile loading in fibre direction is widely regarded to be rate insensitive, however the failure in compression is dependent on the strain rate. The reason is that failure in compression is highly governed by the behavior of the matrix and interface between fibre and matrix.

The data on rate dependent behavior transverse to the fibre direction can be divided into two groups. While one group indicates significant strain rate effects, the other suggests non or only mild rate dependent behavior. It is suggested that such a difference arises due to the strong dependency of the results on the testing method or specimen geometry. The behavior is largely believed to be similar to epoxy resin behavior mentioned previously. Both the tensile and compressive material properties seem to follow this trend the best.

The available data on out of plane shear suggests that it is not governed by the strain rate. This is quite surprising as the failure mode associated with inter-laminar shear stress between plies i.e., delamination, is basically a failure of the matrix in the interface between the plies, which is understood to be rate dependent.

2.6 Summary

In this chapter, a brief historical overview on the various failure theories for unidirectional reinforced composites was presented. The initial part dealt with the initiation criteria for the failure modes of fibre failure, matrix failure and delamination as has been recorded in literature. Specific contributions to fibre kinking brought the approach of considering a kink plane to define the damage criteria into focus. This has led to a different scheme of applying failure criteria to damage planes for the other

intra-laminar failure modes. The other scheme continues to apply the failure criteria based on stresses and their interactions, which are predominantly quadratic in nature as this has found to match experimental results quite well.

The topic of damage evolution for the failure modes was dealt next. It was seen that they range from simple time step based schemes to strain rate based approaches. Some of these schemes are implemented in commercial softwares used in field of Finite Element Analysis (FEA). These schemes belong to either the Fracture mechanics or the Continuum damage mechanics (CDM) approach. It was seen that CDM approach is very suitable for the intra-laminar failure modes. However, for delamination mode, a Fracture mechanics approach seems more suitable, especially with development of cohesive zone models consisting of de-cohesive elements. This approach is thermodynamically consistent as it takes into account the energy release rates and appear physically appropriate.

In the next chapter, a detailed account is given regarding the specific damage model used within this body of work and the implementation details.

Chapter 3

Damage Model

This chapter presents the modelling framework chosen in this body of work to simulate damage for general three dimensional stress states in unidirectional carbon fibre reinforced polymers (CFRP). In the first part, key aspects of the failure model and initiation criteria are introduced. In the second part, damage evolution strategy and damage coupling effects are detailed. This is followed up with the actual implementation in **ABAQUS/Explicit**.

3.1 Introduction

The damage model chosen for implementation is a three dimensional mixed-mode damage model that describes the elastic-brittle behavior of CFRP. Damage in composite materials is represented by two main strategies, micro mechanical modelling and Continuum Damage Mechanics (CDM). Micro mechanical models focus on explicit modelling of damage entities such as voids, matrix cracks, broken fibre filaments etc., using fracture mechanics, while Continuum damage mechanics (CDM) uses a homogenized approach where the local effect of damage is smeared out over the representative volume entity (RVE). In this body of work, macroscopic modelling of composites as a continuum is undertaken and hence, CDM approach is employed. Physically based failure criteria are chosen to initiate damage corresponding to the

failure modes as described previously (see Chapter 2).

Impact damage on composite laminates is a complex phenomena, which includes dynamic structural behavior and loading, contact, friction, damage and failure. CDM is an accurate framework to predict the process of failure of composites. The gradual unloading of a ply after the onset of damage is simulated by means of a material degradation model. The constitutive law is defined using an orthotropic constitutive tensor.

The complex three dimensional stress state resulting out of an impact event cannot be adequately modelled by many failure theories due to the assumption of plane stress. In the present work, *failure criteria* based on three-dimensional stress states are used to predict the material behavior deviating from the linear elastic behavior due to the evolution of damage within the material. These criteria are hence, aptly referred to as *damage initiation criteria* also, which is interchangeably used with the term *failure criteria* in the composite community.

As concluded from the *World Wide Failure Exercise(WWFE)*, physically based failure criteria enable a more accurate prediction of damage evolution since they are based on the underlying physical phenomenon. The chosen physically based failure criteria strictly incorporate only the stress terms that influence a given failure mode.

It is important at this stage to consider the following assumptions pertaining to the model:

- The theoretical basis for the constitutive model of each uni-directional laminate is provided by a homogenized continuum.

- The rules of mixture lead to the elasticity moduli and strength parameters of the undamaged uni-directional laminate, calculated from the properties of the fibre and resin data together with the volume ratios of fibers and matrix.

- The laminate is assumed to have a linear-elastic behavior when loaded, until the initiation of damage. Thereafter, the behavior is non-linear depending on the evolution of the damage variables.

- The orthotropic nature of the laminate as a homogenized continuum is maintained throughout the damage process i.e., the defects in the composite material are treated in the mathematical model as having the equivalent effect on the elastic properties as disc-like cracks would exert, if they are only oriented either tangential or normal to the fibre direction. Therefore, the symmetry class of the uni-directional laminate remains the same for all states of damage.

- After an initial elastic behavior, there is rearrangement of the material properties due to progressive damage.

3.2 Damage Initiation

The formulation used to simulate the damage phenomenon occurring in the out-of-plane, low velocity impact scenario considered in this thesis uses a CDM model for both the inter-laminar and intra-laminar damage. For each damage mode, the constitutive model used in this body of work follows the general form schematically represented in Fig. 3.1. The material response is linear-elastic until the onset of damage and, at higher strains, it softens according to the evolution scheme.

All failure criteria within this thesis are introduced as a measure of the admissibility of the damage surface in stress space, denoted by f. The trespassing of the damage surface indicates the onset of damage for that particular mode, represented by the condition

$$f \geq 1 \tag{3.1}$$

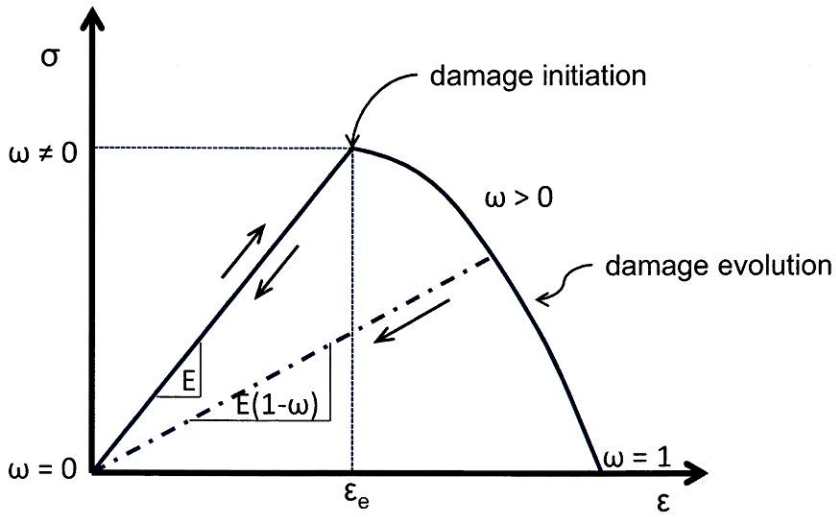

Figure 3.1: Schematic of the damage model

The following composite failure modes are considered in the model

- *Fibre rupture*
- *Fibre crushing*
- *Matrix failure*
- *Delamination*

It was pointed out in Section 2.3.1 that the stress criterion proposed by Hashin (Hashin, 1980) is commonly used in the composites community. A quadratic interaction between the normal and shear stresses for a 3D state of stress is considered towards failure. The intra-laminar failure modes i.e., fibre failure and matrix failure are detected by considering the following failure criteria of Hashin.

For Fibre rupture:

$$\left(\frac{\sigma_{11}}{X_t}\right)^2 + \left(\frac{\sigma_{12}}{S_{12_f}}\right)^2 + \left(\frac{\sigma_{13}}{S_{13_f}}\right)^2 = 1 \quad for \quad \sigma_{11} \geq 1 \tag{3.2}$$

For Fibre crushing:

$$\left(\frac{\sigma_{11}}{X_c}\right)^2 + \left(\frac{\sigma_{12}}{S_{12_f}}\right)^2 + \left(\frac{\sigma_{13}}{S_{13_f}}\right)^2 = 1 \quad for \quad \sigma_{11} < 1 \tag{3.3}$$

For Matrix cracking:

$$\left(\frac{\sigma_{22}}{Y_t}\right)^2 + \left(\frac{\sigma_{12}}{S_{12_m}}\right)^2 + \left(\frac{\sigma_{23}}{S_{23_m}}\right)^2 = 1 \quad for \quad \sigma_{22} \geq 1 \tag{3.4}$$

For Matrix crushing:

$$-\left(\frac{\sigma_{22}}{2\,S_{12_m}}\right)^2 + \left(\left(\frac{Y_c}{2\,S_{12_m}}\right)^2 - 1\right)\frac{\sigma_{22}}{Y_c} + \left(\frac{\sigma_{23}}{S_{23_m}}\right)^2 = 1 \quad for \quad \sigma_{22} < 1 \tag{3.5}$$

The strengths X_t and X_c are obtained from simple uniaxial tensile and compressive tests respectively. The fiber strengths S_{12_f} and S_{13_f} mark fibre failure due to pure shear loading. The shear strength property is not easy to measure as it is difficult to observe experimentally due to its nature. As the uni-directional ply is assumed to be transversally isotropic, no distinguishable differences arise between the fibre shear strengths. Therefore, the following simplification is used

$$S_{12_f} = S_{13_f} = S_f \tag{3.6}$$

The strengths Y_t and Y_c are also obtained from uniaxial tests. The in-plane shear strength S_{12_m} is obtained from pure shear experiment. However, it is mentioned in literature that uniaxial reinforced CFRP when subjected to a pure transverse shear loading (σ_{23_m} acting alone) fail under an angle of $\theta = 45°$. Hence, it is noted that the transverse shear strength reported from uniaxial tests may not be the true shear strength.

Prediction of delamination is based on another stress-based failure criteria. A Frac-

ture Mechanics based approach would be more accurate, but it requires the knowledge of the existence and size of initial defects and use of cohesive zone model with decohesive elements. This was found difficult to include in the FE model and analysis program. Though stress-based criteria usually suffer from mesh dependency problems, this was addressed to some extent by performing a ply level modelling.

For delamination failure mode, the Brewer-Laglace delamination criteria modified with the contribution from Hou (Hou et al., 2001) is used. It reads

$$\begin{aligned} \left(\frac{\sigma_{33}}{Z_t}\right)^2 + \left(\frac{\sigma_{13}+\sigma_{23}}{S_d}\right)^2 &= 1 \text{ for } \sigma_{33} \geq 0 \\ \left(\frac{\sigma_{13}+\sigma_{23}}{S_d}\right)^2 - 8\left(\frac{\sigma_{33}}{S_d}\right)^2 &= 1 \text{ for } -\sqrt{\frac{(\sigma_{13}^2+\sigma_{23}^2)}{8}} \leq \sigma_{33} < 0 \end{aligned} \tag{3.7}$$

The shear strength S_d in both the transverse directions is chosen to be identical, since the interface layer is seen as a resin rich layer, which does not show any directional dependence. This seems like a simplification since it has been reported in studies (Tao and Sun, 1998) that delamination propagation highly depends on the ply orientation of the neighboring plies. The strength properties then, will depend in the ply orientations and probably not identical.

Since the scope of this body of work is limited, no experimental program has been conducted to derive or deduce accurate material properties and logical assumptions wherever applicable, have been made. The material properties used in the above mentioned criteria are taken from available literature alone.

3.3 Damage Evolution

The CDM model used relies on a representation of the damage by introducing a set of internal damage variables and a damage tensor, which is applied to the stiffness

tensor. The internal damage variables as functions of strain rate are introduced into the model and establish relation between damage variables and elastic coefficients. Two measures of stress are introduced, applied macroscopic stress $\boldsymbol{\sigma}$ and effective stress $\hat{\boldsymbol{\sigma}}$. The applied macroscopic stress represents an averaged stress over damaged and undamaged regions within the RVE and is the relevant stress measure from a macroscopic point of view. Effective stress is the stress acting on the cross-section, which is effectively resisting the applied load. The applied and effective stresses are defined as

$$\begin{aligned} \boldsymbol{\sigma} &= \boldsymbol{C}(\boldsymbol{\omega})\boldsymbol{\epsilon} \\ \hat{\boldsymbol{\sigma}} &= \boldsymbol{C^0}\boldsymbol{\epsilon} \end{aligned} \tag{3.8}$$

where, $\boldsymbol{C^0}$ refers to the undamaged stiffness tensor and $\boldsymbol{C}(\boldsymbol{\omega})$ denotes the damaged stiffness tensor.

Based on the approach of strain equivalence, the relation between applied stress and effective stress can be expressed as

$$\boldsymbol{\sigma} = \boldsymbol{M}(\boldsymbol{\omega})\hat{\boldsymbol{\sigma}} \tag{3.9}$$

where, $\boldsymbol{M}(\boldsymbol{\omega})$is a transformation tensor as a function of the damage state $\boldsymbol{\omega}$. Introducing the stress-strain relationship (Equation (3.8)) into Equation (3.9) yields

$$\boldsymbol{\sigma} = \boldsymbol{M}(\boldsymbol{\omega})\boldsymbol{C^0}\boldsymbol{\epsilon} = \boldsymbol{C}(\boldsymbol{\omega})\boldsymbol{\epsilon} \tag{3.10}$$

The propagation of damage is entirely driven by the rate at which certain failure surfaces are exceeded. The failure criteria introduced in Equation (3.2)-Equation (3.5) and Equation (3.7) earlier are used as the definition of surfaces in stress space i.e., f. The respective damage variables and consequent stress reduction is obtained by considering the variation of the surfaces in strain space, denoted by g. Damage is

represented by a growth of the failure surface thus shrinking the domain where the material remains elastic.

The current implementation uses the damage model proposed by Matzenmiller (Matzenmiller et al., 1995) for plane stress formulation and later extended to three dimensions by Curiel Sosa (Curiel et al., 2008). The damage modes are represented by a set of state variables (damage variables) ω_{ij} that represent the state of damage in the composite for that particular mode. The indices ij correspond to the principal stress responsible for the presence of the particular damage mode. The rate of evolution of damage variables is assumed to be locally governed by the local state variables $\boldsymbol{\sigma}$, $\boldsymbol{\omega}$. The rate-equations for the damage variables ω_{ij} - denoted as the *"damage rule"* - allow independent growth of the damage parameters or appropriate coupling among them. The damage rule $\dot{\boldsymbol{\omega}}(\boldsymbol{\sigma}, \boldsymbol{\omega}, \dot{\boldsymbol{\epsilon}})$ is defined as a linear combination of the growth functions and the damage directors

$$\dot{\boldsymbol{\omega}} = \mathrm{f}(\phi_i, \mathbf{q}_i) \tag{3.11}$$

where, i denotes a mode of damage. The scalar damage growth functions $\phi_i(\boldsymbol{\sigma}, \boldsymbol{\omega}, \dot{\boldsymbol{\epsilon}})$ defined for each damage mode, control the amount of growth and the vector-valued functions $\mathbf{q}_i(\boldsymbol{\sigma}, \boldsymbol{\omega})$ (damage directors) accommodate the coupling of growth for the individual damage variables in the various damage modes. It is assumed that the coupling among the damage variables through $\mathbf{q}_i$ is independent of the strain-rate itself. The growth function for each of the damage modes is computed through the relation

$$\phi_i = \langle \nabla_\epsilon g_i / \| \nabla_\epsilon g_i \|, \dot{\boldsymbol{\epsilon}} \rangle_+ \tag{3.12}$$

where, ∇_ϵ denotes the strain gradient $\frac{\partial}{\partial \epsilon}$ and $\dot{\boldsymbol{\epsilon}}$ the strain rate. g_i are the evolving damage surfaces in the strain space. $\langle \cdot \rangle_+$ is the non-negative inner product, vanishing for negative values, thus here accounting for the trespassing on the damage surface.

The inner product norm between the strain rate $\dot{\boldsymbol{\epsilon}}$ and the normal to the level

curves of the loading surface $\nabla_\epsilon g$ has geometrical significance. The strain increment $\dot{\boldsymbol{\epsilon}}\, dt$ indicates the direction of the loading path $\boldsymbol{\epsilon}$ as it crosses the loading surface $g = 0$ in strain space. The scalar $\phi_i \geq 0$ has to be associated with each loading direction $\dot{\boldsymbol{\epsilon}}$ in relation to the orientation of the normal $\nabla_\epsilon g$ and is in accordance with the following conditions:

(i) $\phi_i = 0$ when $g_i \leq 0, f_i \leq 0$, where g_i and f_i are surfaces in strain and stress space respectively.
The strain path is in the interior of the elastic range ε or comes into contact with the boundary $\partial\varepsilon$.

(ii) $\phi_i > 0$ when $g_i = 0_+, f_i = 0_+$, where g_i and f_i are surfaces in strain and stress space respectively.
The strain path crosses the loading surface $f_i = 0, g_i = 0$, indicated by the "+" sign at the end of the criterion. The strain increment has a non-zero component pointing in the direction of the gradient $\nabla_\epsilon g_i$.

The evolving damage surfaces in the strain space g_i are given by the relation

$$g_i = \boldsymbol{\epsilon}^T \cdot \mathbf{G}_i \cdot \boldsymbol{\epsilon} - c_i \tag{3.13}$$

c_i is an empirical parameter defining the damage surface.

The variations of these surfaces in strain space are given by

$$\nabla_\epsilon g_i = \boldsymbol{\epsilon}^T \cdot (\mathbf{G}_i^T + \mathbf{G}_i) \tag{3.14}$$

where, $\mathbf{G}_i$ are second order tensors in strain space derived from the constitutive law in Equation (3.10) and from the following equivalence of quadratic forms in stress and strain spaces

$$\boldsymbol{\sigma}^T \cdot \mathbf{F}_i \cdot \boldsymbol{\sigma} = \boldsymbol{\epsilon}^T \cdot \mathbf{G}_i \cdot \boldsymbol{\epsilon} \tag{3.15}$$

The second order tensors in stress space $\mathbf{F}_i$ are derived from stress-based criteria of failure defined in Section 3.2 with the introduction of damage variables ω_{ij}. The modelling of damage directors $\mathbf{q}_i$ is based on stiffness components that are degraded when a particular mode of damage occurs. For example, fibre rupture $\mathbf{q}_1$ affects the stiffness degradation in 11, 12 and 13 directions. This is represented by weights λ in the vector $\mathbf{q}_1$ as shown in Equation (3.16)

$$\mathbf{q}_1 = [\lambda_{11}\ 0\ 0\ \lambda_{12}\ 0\ \lambda_{13}] \tag{3.16}$$

The damage directors $\mathbf{q}_i$ allow coupling between the damage variables. The weights λ are estimated values associated with a particular mode of failure and further work needs to be taken up to calibrate them. In this body of work, it was seen that the best results were obtained when the damage directors were assigned unitary weights corresponding to the principal stresses associated with a particular mode of failure. An over prediction of damage region was observed with the form of damage director as in Equation (3.16). Hence, in this thesis the simulation results in Chapter 4 are presented with a simplified form of the damage director. For example, fibre rupture $\mathbf{q}_1$ caused primarily by the principle stress $\boldsymbol{\sigma_{11}}$ is given the following form

$$\mathbf{q}_1 = [1\ 0\ 0\ 0\ 0\ 0] \tag{3.17}$$

However, there are shortcomings with this approach as pointed out later in Section 5.2. The coupling between additional stress terms is defined through the damage variables in the definition of the second order tensors $\mathbf{F}_i$.

3.4 Damaged Stiffness Tensor

The macroscopic (damaged) stress $\boldsymbol{\sigma}$ is calculated from the constitutive law and the current state of damage. Hence, the current state of damage has to be incorporated

into the stiffness tensor $\boldsymbol{C}$. Within the framework of CDM, the effective stress $\hat{\boldsymbol{\sigma}}$ (stress acting on the undamaged cross section of the RVE) is related to the applied macroscopic stress $\boldsymbol{\sigma}$ (using Voigt-Kelvin notation) by

$$\boldsymbol{\sigma} = \boldsymbol{M}\hat{\boldsymbol{\sigma}} \tag{3.18}$$

where,

$$\boldsymbol{\sigma}^T = \begin{bmatrix} \sigma_{11} & \sigma_{22} & \sigma_{33} & \sigma_{12} & \sigma_{23} & \sigma_{31} \end{bmatrix} \tag{3.19}$$

and $\boldsymbol{M}$ is the stiffness damage tensor represented as

$$\boldsymbol{M} = diag\begin{bmatrix} (1-\omega_{11}) & (1-\omega_{22}) & (1-\omega_{33}) & (1-\omega_{12}) & (1-\omega_{23}) & (1-\omega_{31}) \end{bmatrix} \tag{3.20}$$

Equation (3.18) can be rewritten as

$$\boldsymbol{\sigma} = \boldsymbol{M}\boldsymbol{C}^0\boldsymbol{\epsilon} = \boldsymbol{C}(\boldsymbol{\omega})\boldsymbol{\epsilon} \tag{3.21}$$

and yields the damaged stiffness tensor $\boldsymbol{C}(\boldsymbol{\omega})$

$$\boldsymbol{C}(\boldsymbol{\omega}) = \begin{pmatrix} (1-\omega_{11})C_{11} & (1-\omega_{11})C_{12} & (1-\omega_{11})C_{13} & 0 & 0 & 0 \\ (1-\omega_{22})C_{12} & (1-\omega_{22})C_{22} & (1-\omega_{22})C_{23} & 0 & 0 & 0 \\ (1-\omega_{33})C_{13} & (1-\omega_{33})C_{23} & (1-\omega_{33})C_{33} & 0 & 0 & 0 \\ 0 & 0 & 0 & (1-\omega_{12})C_{44} & 0 & 0 \\ 0 & 0 & 0 & 0 & (1-\omega_{23})C_{55} & 0 \\ 0 & 0 & 0 & 0 & 0 & (1-\omega_{31})C_{66} \end{pmatrix} \tag{3.22}$$

The matrices $\boldsymbol{A}$ and $\boldsymbol{B}$ defined in a local system of reference are introduced in

order to read $\boldsymbol{C}$ in a more compact manner with the constituents, such that

$$\boldsymbol{C}(\boldsymbol{\omega}) = \left[\begin{array}{c|c} \boldsymbol{A}(\boldsymbol{\omega}) & 0 \\ \hline 0 & \boldsymbol{B}(\boldsymbol{\omega}) \end{array}\right] \tag{3.23}$$

where,

$$\boldsymbol{A}(\boldsymbol{\omega}) = \begin{bmatrix} \frac{(1-\omega_{11})(1-\nu_{23}\nu_{32})}{E_{22}E_{33}\Delta} & \frac{(1-\omega_{11})(\nu_{12}+\nu_{32}\nu_{13})}{E_{11}E_{33}\Delta} & \frac{(1-\omega_{11})(\nu_{13}+\nu_{12}\nu_{23})}{E_{11}E_{22}\Delta} \\ \frac{(1-\omega_{22})(\nu_{12}+\nu_{32}\nu_{13})}{E_{11}E_{33}\Delta} & \frac{(1-\omega_{22})(1-\nu_{13}\nu_{31})}{E_{11}E_{33}\Delta} & \frac{(1-\omega_{22})(\nu_{23}+\nu_{21}\nu_{13})}{E_{11}E_{22}\Delta} \\ \frac{(1-\omega_{33})(\nu_{13}+\nu_{12}\nu_{23})}{E_{11}E_{22}\Delta} & \frac{(1-\omega_{33})(\nu_{23}+\nu_{21}\nu_{13})}{E_{11}E_{22}\Delta} & \frac{(1-\omega_{33})(1-\nu_{12}\nu_{21})}{E_{11}E_{22}\Delta} \end{bmatrix} \tag{3.24}$$

and

$$\boldsymbol{B}(\boldsymbol{\omega}) = \begin{bmatrix} (1-\omega_{12})G_{12} & 0 & 0 \\ 0 & (1-\omega_{23})G_{23} & 0 \\ 0 & 0 & (1-\omega_{31})G_{31} \end{bmatrix} \tag{3.25}$$

with

$$\Delta = \frac{(1-\nu_{12}\nu_{21}-\nu_{23}\nu_{32}-\nu_{31}\nu_{13}-2\nu_{21}\nu_{32}\nu_{13})}{E_{11}E_{22}E_{33}} \tag{3.26}$$

3.5 VUMAT Formulation

The VUMAT subroutine is called by **ABAQUS/Explicit** at every time step and strain increment passed on along with the damage variables computed in the previous step. The flowchart in Figure 3.2 shows the procedure as implemented in the subroutine. The computations are performed for all the material points in the model. The superscript γ in the chart refers to the damage modes. It allows the computation of $\mathbf{F}$ and $\mathbf{G}$ as a 3rd order tensor for convenience, with the 3rd index γ corresponding to the individual damage mode.

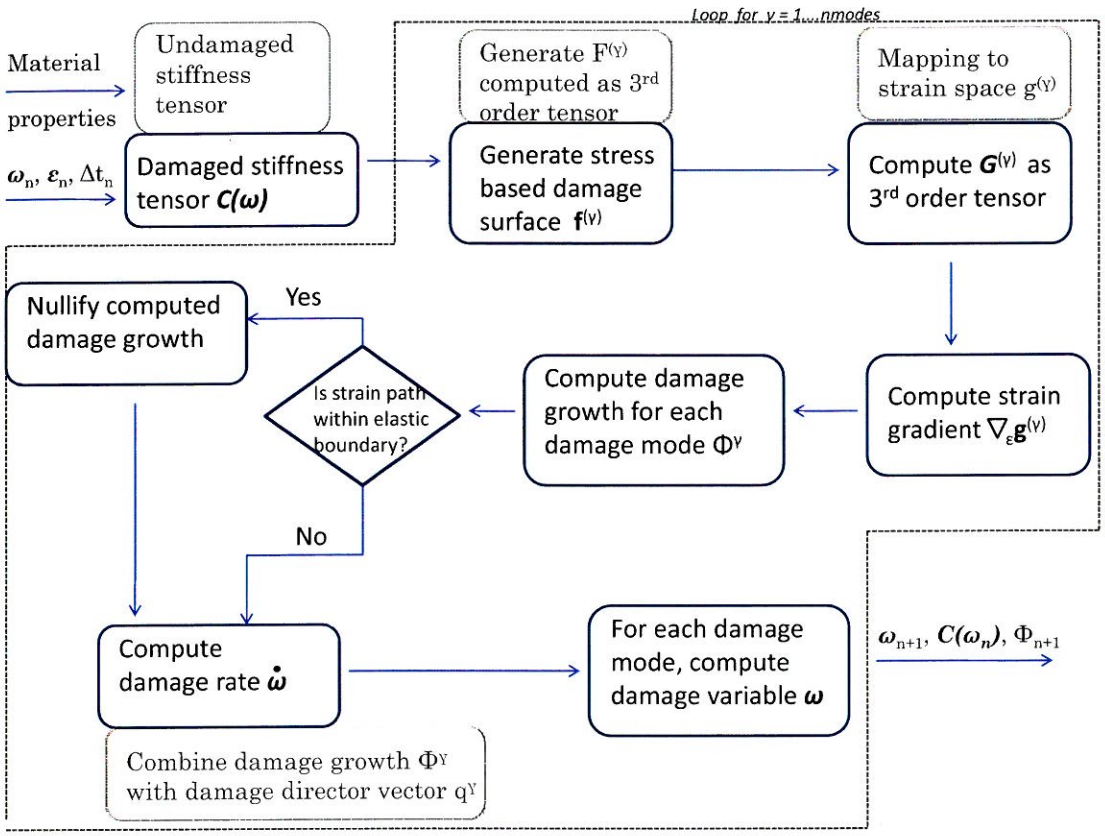

Figure 3.2: Flowchart of steps used in VUMAT

The material properties are entered into the **ABAQUS/Explicit** property module. The damage variables and strain for computation are stored as state defined variables (SDV). These are initialized at the beginning of the explicit scheme and subsequently updated at the end of every time step.

The new strain and stress for the current time step are computed from the strain increment provided by the explicit scheme as

$$\begin{aligned} \boldsymbol{\epsilon}^{N+1} &= \boldsymbol{\epsilon}^{N} + \Delta\boldsymbol{\epsilon} \\ \boldsymbol{\sigma}^{N+1} &= \boldsymbol{C}(\omega) \cdot \boldsymbol{\epsilon}^{N+1} \end{aligned} \tag{3.27}$$

The damage surface in stress space f^{N+1} in the current time step is computed corresponding to the particular damage mode as shown below.

For Fiber failure:

$$f_{\parallel}^{N+1} = \frac{\sigma_{11}^2}{(1-\omega_{11})^2\ X_{11_{t,c}}^2} + \frac{\sigma_{12}^2}{(1-\omega_{12})^2\ S_{12}^2} + \frac{\sigma_{13}^2}{(1-\omega_{13})^2\ S_{13}^2} \tag{3.28}$$

For Matrix cracking:

$$f_{\perp}^{N+1} = \frac{\sigma_{22}^2}{(1-\omega_{22})^2\ X_{22_t}^2} + \frac{\sigma_{12}^2}{(1-\omega_{12})^2\ S_{12}^2} + \frac{\sigma_{23}^2}{(1-\omega_{23})^2\ S_{23}^2} \tag{3.29}$$

For Matrix crushing:

$$f_{\perp}^{N+1} = \frac{-\sigma_{22}^2}{4\ (1-\omega_{22})^2\ S_{12}^2} + \left(\left(\frac{X_c}{2\ S_{12}}\right)^2 - 1\right)\frac{\sigma_{22}}{(1-\omega_{22})\ X_c} + \frac{\sigma_{23}^2}{(1-\omega_{23})^2\ S_{23}^2} \tag{3.30}$$

For Delamination (Tensile stress):

$$f_{\perp\perp}^{N+1} = \frac{\sigma_{33}^2}{(1-\omega_{33})^2\ X_{33}^2} + \frac{\sigma_{23}^2}{(1-\omega_{23})^2\ S_{13}^2} + \frac{\sigma_{13}^2}{(1-\omega_{13})^2\ S_{13}^2} \tag{3.31}$$

For Delamination (Compressive stress):

$$f_{\perp\perp}^{N+1} = \frac{\sigma_{23}^2}{(1-\omega_{23})^2\ S_{13}^2} + \frac{\sigma_{13}^2}{(1-\omega_{13})^2\ S_{13}^2} - 8\ \frac{\sigma_{33}^2}{(1-\omega_{33})^2\ S_{13}^2} \tag{3.32}$$

The formulation for damage surface in stress space as shown in Equation (3.28) to Equation (3.32) allows for the computation of the second order tensor $\mathbf{F}$. Then, the second order tensor $\mathbf{G}$ in strain space can be computed from the equivalence of

quadratic forms in stress and strain space (Lemaitre and Chaboche, 1978) given by

$$\boldsymbol{\sigma}^T \cdot \mathbf{F} \cdot \boldsymbol{\sigma} = \boldsymbol{\epsilon}^T \cdot \mathbf{G} \cdot \boldsymbol{\epsilon} \tag{3.33}$$

Thus, the second order tensor $\mathbf{G}^{N+1}$ in strain space in the current time step is computed as

$$\mathbf{G}^{N+1} = \boldsymbol{C}(\boldsymbol{\omega})^T \cdot \mathbf{F} \cdot \boldsymbol{C}(\boldsymbol{\omega}) \tag{3.34}$$

The variation of the damage surface in strain space (gradient to strain surface) $\nabla_\epsilon g$ is computed as

$$\nabla_\epsilon g = \boldsymbol{\epsilon}^{N+1} \cdot \left((\mathbf{G}^{N+1})^T + \mathbf{G}^{N+1}\right) \tag{3.35}$$

The growth function ϕ^{N+1} in the current time step is computed as

$$\phi^{N+1} = \langle \nabla_\epsilon g_i / \|\nabla_\epsilon g_i\|, \dot{\boldsymbol{\epsilon}} \rangle_+ \tag{3.36}$$

Then, the evolution of damage variable $\dot{\boldsymbol{\omega}}^{N+1}$ is given by

$$\dot{\boldsymbol{\omega}}^{N+1} = \phi^{N+1} \cdot \mathbf{q} \tag{3.37}$$

The damage increment of the current time step $\delta\boldsymbol{\omega}^{N+1}$ is computed as

$$\delta\boldsymbol{\omega}^{N+1} = \dot{\boldsymbol{\omega}}^{N+1} \cdot \delta t \tag{3.38}$$

Finally, the accumulation of damage $\boldsymbol{\omega}^{N+1}$ for the time step is given as

$$\boldsymbol{\omega}^{N+1} = \boldsymbol{\omega}^N + \delta\boldsymbol{\omega}^{N+1} \tag{3.39}$$

3.6 Summary

In this chapter, details concerning the implemented damage model were introduced. The specific damage initiation criteria chosen to detect the failure modes have been provided along with the methodology used for damage evolution. The failure criteria

are stress based with the evolution driven by the rate at which respective failure surfaces are exceeded. The material degradation due to damage growth is performed on the respective driving components thus enabling a physically based representation of the experimentally observed damage.

The following chapter presents the numerical results from the implementation of the routine in **ABAQUS/Explicit** along with the details on the physical model creation.

Chapter 4

Numerical Results

In this chapter, the constitutive model introduced in Chapter 3 is applied to simulate standard impact experiments conducted on composite laminates in aerospace industry. The experiments are referenced from work of Hou (Hou et al., 2001) and Lopes (Lopes et al., 2009a,b), where similar tests were conducted on two different composite laminates. The aim of the modelling exercise is to verify the prediction of damage initiation and evolution with the constitutive model and account its performance.

4.1 Introduction

This section describes the numerical strategy used to model the low-velocity impact tests carried out by Hallett at University of Oxford and Lopes at University of Delft. Hou (Hou et al., 2001) have conducted numerical simulations of Hallett's work in LS-DYNA and compared results.

The purpose of the simulations is to verify the model described in Section 3.3 when combined with appropriate damage detection criteria. The results should not be seen as model validation as considerable work in terms of experimental tests and subsequent calibration of stiffness and strength data and model parameters, is required. The simulations primarily give the confidence in applicability of the model in

low-velocity impact conditions as simulated in the tests.

The simulations of the impact problem in the presented thesis have made use of the **ABAQUS/Explicit** FE code . The developed FE models simulate several physical processes which occur during low-velocity impacts on composite laminates. Effort is put on the correct geometrical representation of the structural system, loads, boundary conditions, material behavior and contact conditions between the bodies involved.

Symmetry boundary conditions in both X-direction and Y-direction are applied to represent 1/4 th geometry model. Only a small portion of the impactor is actually modelled for display purpose, since the rigid body definitions in **ABAQUS/Explicit** allow the properties to be applied to a `Reference point` tied to the geometry. The impact velocity is applied as an initial velocity to the `Reference point` at the beginning of the analysis.

Each laminate ply is modelled with one solid `C3D8R` reduced integration element consisting of a single integration point through the thickness of the ply. The mesh density is kept relatively fine only around the impact zone along the plies instead of the whole plate, to save computational effort. In order to prevent hourglassing of the reduced integration elements, the `stiffness relaxation` option is used. The impactor is discretised with `R3D4` rigid shell elements and the support is modelled using `C3D8R` solid elements. Due to the availability of only a single CPU of a personal computer for the analysis, mass scaling has been used to run the analysis in a reasonable amount of time. The mass of elements around the impact zone has been scaled manually and a fixed time increment forced on **ABAQUS/Explicit** to run the simulations. The time increment was arrived at by trial and error and, chosen such that the computed response throughout the loading history is stable and valid in terms of energy.

Contact conditions are defined between the surfaces using the `general contact`

Damage Mode	Principle stress component	VUMAT variable	ABAQUS/Explicit variable
Fibre failure	σ_{11}	ω_1	SDV1
Matrix failure	σ_{22}	ω_2	SDV2
Delamination	σ_{33}	ω_3	SDV3
Shear contribution	σ_{12}	ω_4	SDV4
Shear contribution	σ_{23}	ω_5	SDV5
Shear contribution	σ_{13}	ω_6	SDV6

Table 4.1: Relation between damage variables (ω) and SDV's in **ABAQUS/Explicit**

`algorithm` available in **ABAQUS/Explicit** with a penalty enforcement contact method. The `tangential contact` model with a friction coefficient of $\mu = 0.3$ is used to define the interaction property. The surfaces are assigned such that the impactor surface is the `master` for impactor-laminate contact and relatively coarsely meshed support surface serves as the `master` for contact between impactor-support. A `tie contact` definition is used in order to ensure that the selected surfaces remain in contact with each other as the simulation progresses.

It was decided to approach the development of the `FORTRAN` routine `VUMAT` for a completely orthotropic model capable of capturing damage modes related to fibre and matrix failure and delamination, along with the interaction between them, in two stages. In the first stage, the `VUMAT` routine was written for an orthotropic material without taking damage evolution into consideration. Upon completion of this stage, damage evolution was incorporated into the model. `State dependent variables (SDV)` available in **ABAQUS/Explicit** are used to monitor the damage associated with a particular damage mode. Each SDV in the output plot represents a particular damage variable. For example, damage variable associated with delamination ω_3 in `VUMAT` is represented by SDV3 in **ABAQUS/Explicit**. Table 4.1 provides clarity into this aspect of result processing.

The results from the numerical simulation work carried out in this thesis are compared against the experimental results to provide some insight into the general capability of the model. Qualitative results of the damage region after impact in test specimens were observed after subjecting them to ultrasonic C-scan and sectioning through the centre of the damage region in the direction of short axis. In order to overcome the obvious limitations of inspecting the damaged zone due to lack of image contrast, a *Liquid Penetrant Inspection Technique*, based on capillary action was used. The cut sections were dipped in a dye that fluoresces when excited by ultraviolet radiation. An image of the specimen section is then available for processing. The focus was on damage caused by delamination mode in the laminates under a low-velocity impact. Quantitative results wherever available are compared for drawing inference regarding shortcomings and better calibration requirements of the model. The following sections present the sequential methodology adapted to develop the final model.

4.2 Single element tests

Single element test results with the modified routine are presented in Fig. 4.1 for uni-axial tension and compression tests. Damage initiation occurs for only those damage variables which are associated with the principal stress in the direction of applied load. Since, no direct coupling was enforced through the damage directors, damage is accumulated only by single damage variables in each direction. Once damage is detected, evolution of the damage variable takes place at a rate depending on the strain rate. The slope of the straight line represents the rate of evolution of the damage variable. Faster the strain rate, steeper is the slope and earlier is the point of damage detection. This effect can be observed by comparing Fig. 4.1a-Fig. 4.2a, and Fig. 4.1b-Fig. 4.2b. For a higher prescribed displacement in the same time interval, damage initiation happens earlier as more damage is accumulated. The difference in the damage evolution plots verify the strain rate dependent formulation of the model. The stress strain plots in the fibre and transverse direction confirm the progressive

nature of the model. Damage detection leads to a departure from the linear elastic path after the corresponding strength in that direction is reached. A certain amount of strain is accumulated before all the strength is lost.

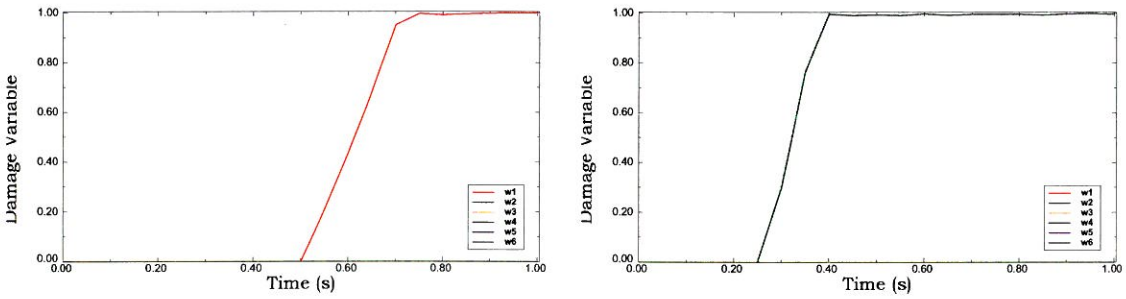

(a) Damage variable evolution in fibre direction **(b)** Damage variable evolution in transverse direction

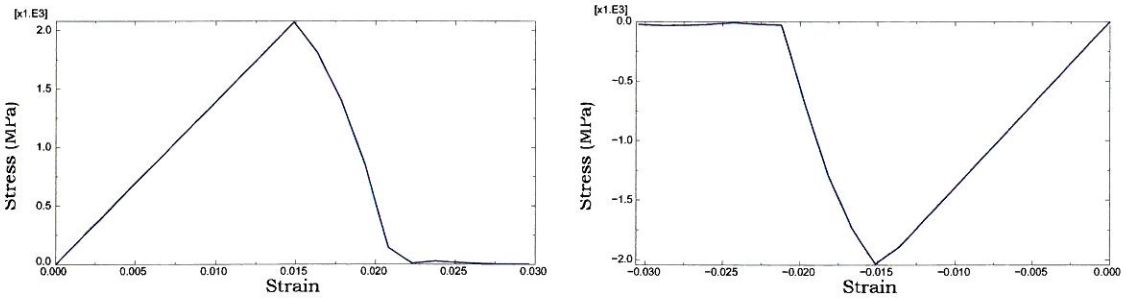

(c) σ_{11} vs ϵ_{11}-Tension **(d)** σ_{11} vs ϵ_{11}-Compression

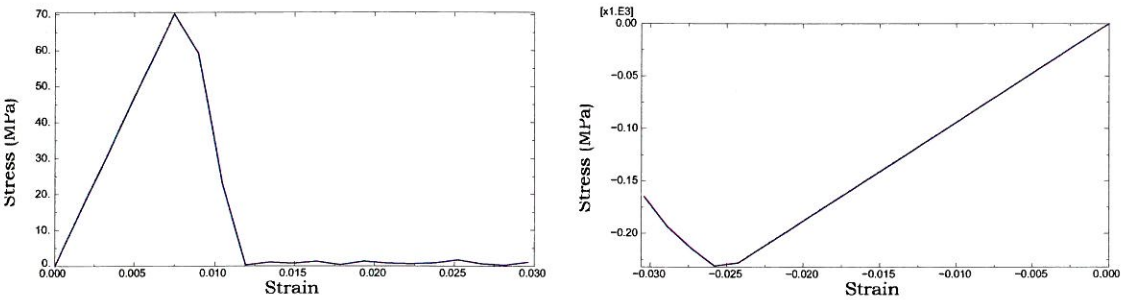

(e) σ_{22} vs ϵ_{22}-Tension **(f)** σ_{22} vs ϵ_{22}-Compression

Figure 4.1: Uniaxial tension and compression results for single element at strain rate $\dot{\epsilon} = 0.03\ s^{-1}$

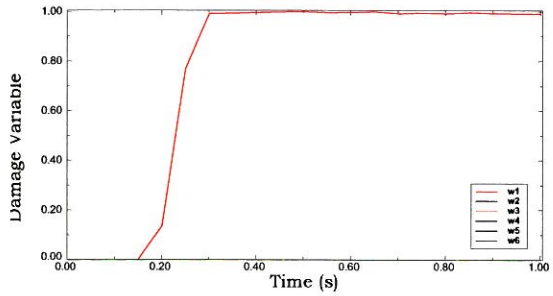

(a) Damage variable evolution in fibre direction

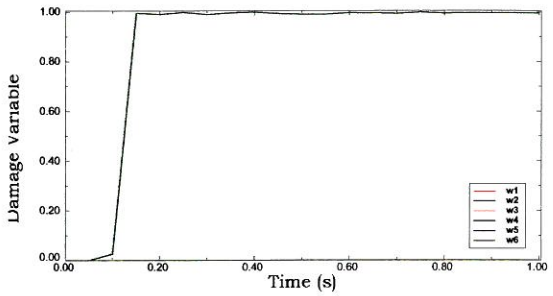

(b) Damage variable evolution in transverse direction

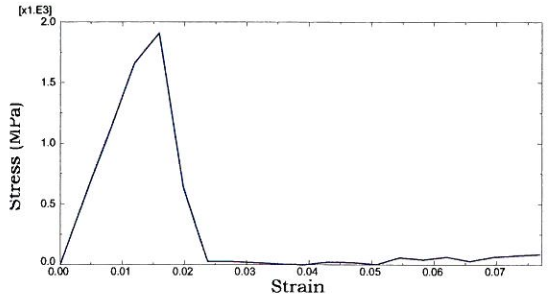

(c) σ_{11} vs ϵ_{11}-Tension

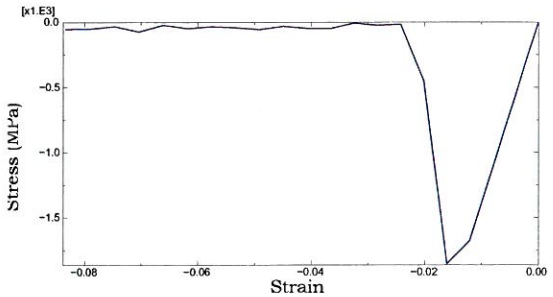

(d) σ_{11} vs ϵ_{11}-Compression

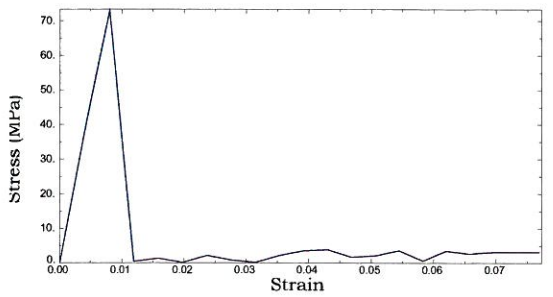

(e) σ_{22} vs ϵ_{22}-Tension

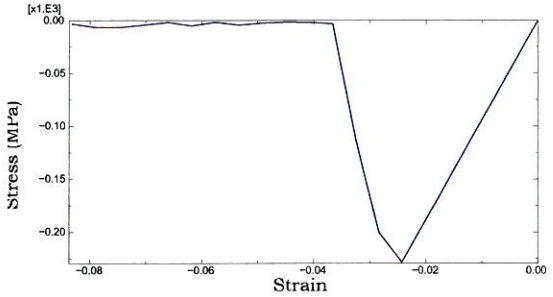

(f) σ_{22} vs ϵ_{22}-Compression

Figure 4.2: Uniaxial tension and compression results for single element at strain rate $\dot{\epsilon} = 0.08\ s^{-1}$

4.3 Hallett experiment

The experiment by Hallett was carried out using a gas gun apparatus as shown in Fig. 4.3. To ensure that the test geometry was the same as used by the aerospace industry (Airbus Industrie Test Method 1.0010, 1993; Boeing Advanced composite tests,

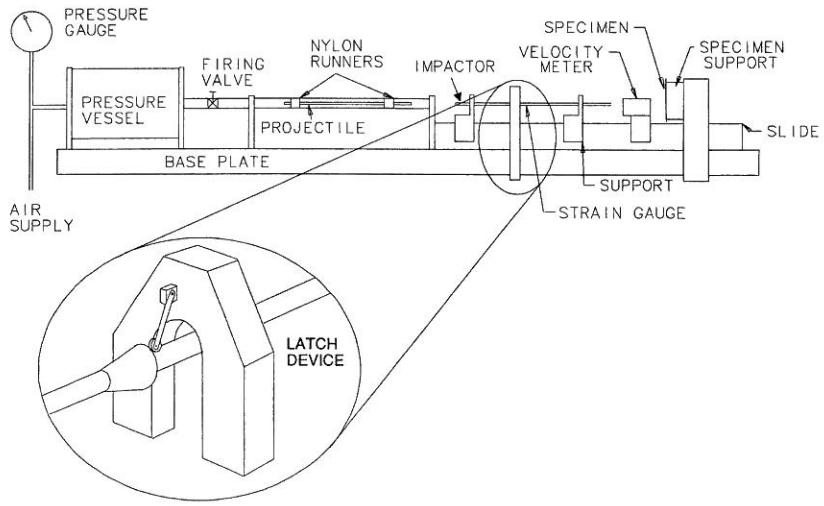

Figure 4.3: Set-up of the gas gun apparatus (Hou et al., 2001)

1998), the impactor was fitted with a spherically ended steel cap 16 mm in diameter and rubber bungs were used to damp the oscillations in the force signal. The impactor was fired with an initial velocity of 7.08 ms^{-1} resulting in an impact energy of 6.5 J. The total mass of the impactor was 260 g. In the test, the titanium projectile launched by the gas gun hits the impactor, which then strikes the composite specimen. The distance between the impactor and the specimen was sufficient to ensure that the former was in a stress-free state on impact. A latch device was fitted so as to avoid multiple impacts when the impactor bounced off the specimen. The velocity of the impactor was measured by infra-red timing gates just before it struck the specimen.

The dimensions of the composite plate tested were 140 x 85 x 2.6 mm^3. The material tested was unidirectional CFRP T300/914 with a fibre volume fraction of 0.6. Layup of the composite plate used was 21 plies of [0°/90°] alternate with the direction of the fibre in the outermost plies along the longer side of the plate i.e along global material 1-direction. The impactor was a titanium alloy rod 9.55 mm in diameter and 500 mm in length. The plate was simply supported by a support block containing a 45 mm diameter circular hole at the centre (see Fig. 4.4).

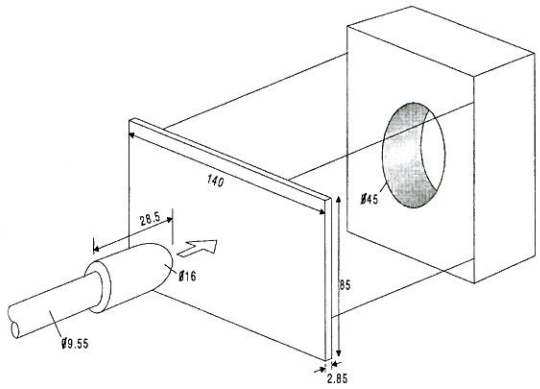

Figure 4.4: Geometry of plate and support (Hou et al., 2001)

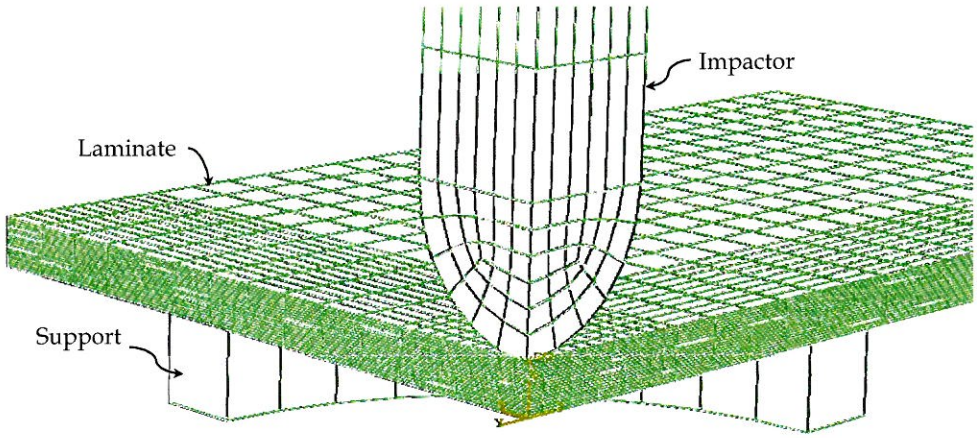

Figure 4.5: Mesh of the plate model for Hallet's experiment

4.3.1 Physical Model

In the simulations, the composite plate is modelled as a 21 section plate; each section representing a laminate ply with alternate [0°/90°] material orientations assigned to the sections. Material data available from (Hou et al., 2001) and presented in Table 4.2 are applied as composite material properties. The support is modelled as an elastic isotropic material (steel) with a diameter of 45 mm, fixed and simply supporting the plate. The impactor is modelled as a rigid body with a lumped mass equal to 260 g as used in the experiments. The analysis was run for a step time of 1 ms. Overall, the increase of the total mass of the model was kept below 1.3%.

Property	Value	Units
Young's modulus in the fibre direction E_1	139	GPa
Young's modulus in the transverse direction E_2	9.4	GPa
Young's modulus in the through-thickness direction E_3	9.4	GPa
Poisson's ratio ν_{12}	0.0209	
Poisson's ratio ν_{23}	0.33	
Poisson's ratio ν_{13}	0.0209	
Shear modulus G_{12}	4.5	Gpa
Shear modulus G_{23}	2.98	Gpa
Shear modulus G_{13}	4.5	Gpa
Tensile strength in the fibre direction X_T	2070	Mpa
Tensile strength in the transverse direction Y_T	74	Mpa
Compressive strength in the transverse direction Y_C	237	Mpa
Tensile strength in the through-thickness direction Z_T	94	Mpa
Shear strength concerning fibre failure S_f	120	Mpa
Shear strength concerning matrix cracking S_m	86	Mpa
Shear strength concerning delamination S_d	86	Mpa
Mass density ρ	1580	kg m^{-3}

Table 4.2: Composite material properties of UD CFRP T300/914 with $\nu_f = 0.6$ (Hou et al., 2001)

4.3.2 Results

Experimental

Fig. 4.6 shows the delamination of the plate after impact, detected by a dye penetrant, in the experiment of Hallett after sectioning. The light colour corresponds to delamination with a damage free region just under the impact zone clearly visible. Only qualitative results in the form of damage patterns are available for comparison. Impactor reaction force plots were not presented in (Hou et al., 2001) regarding the experiments.

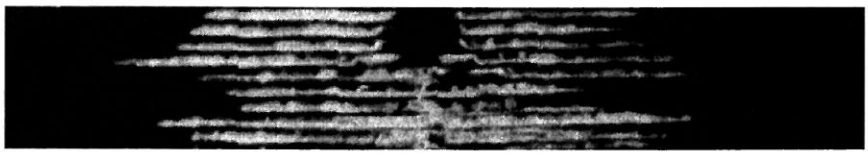

Figure 4.6: Delamination region in Hallett experiment (Hou et al., 2001)

Simulation

(a) Orthotropic Model Without Damage Evolution

The `VUMAT` routine is formulated with damage variables $\omega_1 \cdots \omega_6$, which explicitly monitor the damage associated with the corresponding stress component and hence, indicate presence of that particular mode of failure. The damage variable is set to accept a value of either 0 or 1 (restricted to 0.99 in order to avoid division by zero in the calculations) depending on the satisfaction of the detection criteria (refer Section 3.2).

The routine when applied to the FE model representing Hallett's experiment shows the delamination damage pattern presented in Fig. 4.7. A damage free region can be seen right below the impactor. The damage is seen to progress along the central plies as expected since the shear stresses peak in these regions and are the main contributors to the normal stress, resulting in release of accumulated energy in the form of delamination failure. Damage can also be observed in plies farthest from the impact surface directly under the impactor as has been observed in the experimental results in Fig. 4.6.

(b) Orthotropic Model with Damage Evolution

Verification of the model through the single element tests provides a good confidence in the capability of the model when applied to FE models representing

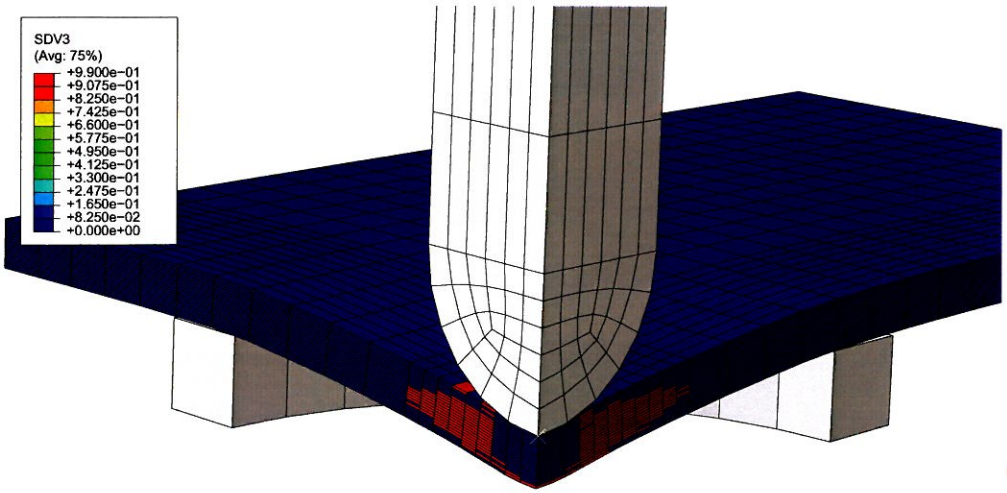

Figure 4.7: Predicted delamination damage using `VUMAT` with $\dot{\omega} = 0$

the experimental cases. Application of the `VUMAT` routine to FE model representing Hallett's experiment provides delamination damage patterns as shown in Fig. 4.9. Damage is detected at a very early stage around the impact point due to high local stresses. High shear stresses in the middle plies leads to damage initiation after about $t = 0.15$ ms. The damage zone progresses along the neutral plane of the laminate maintaining more or less a symmetrical pattern. Extensive damage in the middle plies is seen by $t = .625$ ms into the simulation. The damage pattern retains the shape after this point of time. Some additional damage on the top ply surface is seen which was not reported in the experimental plot and in Hou's simulation results. These could be attributed to non-calibration of the model and influence of other damage modes due to the mixed mode nature of the model. However, the delamination damage pattern bears close resemblance with the damage predicted by Hou in Fig. 4.8. Comparing with the experimental results of Hallett in Fig. 4.6, a characteristic damage free region can be seen under the impact zone. Only the bottommost plies show some damage in line with the experimental plots. Overall, the simulated damage pattern is comparable with the qualitative damage plots obtained from the

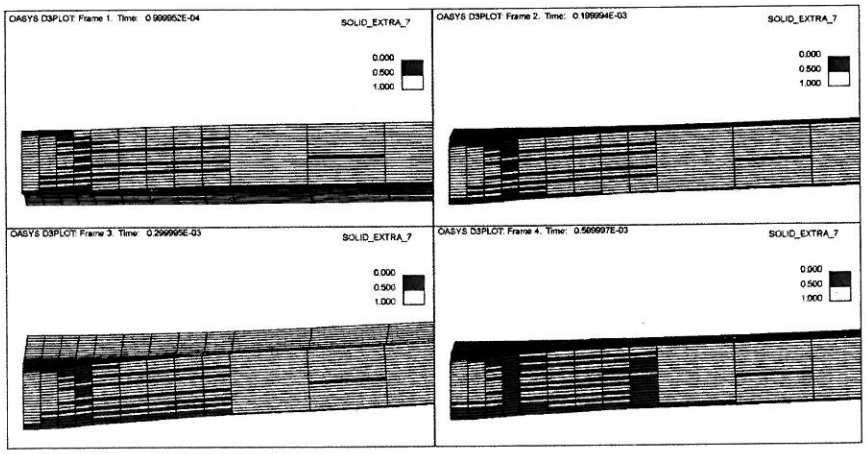

Figure 4.8: Predicted delamination by Hou (Hou et al., 2001)

experiments and simulation results of Hou for a similar mesh.

Quantitative results in the form of impactor reaction force plots were obtained from the simulation for better understanding of the impact dynamics. The plotted quantities were extracted from the `Reference Point` corresponding to the tip of the impactor. Fig. 4.10 presents the variation of the impactor reaction force over time and the corresponding displacement of the tip. The peaks in the plot correspond to occurrence of damage. Considerably sized delaminations are seen to occur at a force of 2 kN. This is seen to occur at around 0.4 ms after impact and corresponding to around 2.8 mm deformation. A gradual delamination growth is actually seen to occur starting at $t = 0.3$ ms. Due to the non-availability of force histories from experimental tests of Hallett, a direct comparison is not possible. However, the general trend predicted by the numerical simulation is well representative of the results from such an experimental test with an oscillatory behaviour due to the dynamic coupling between the specimen and its supports. The maximum impactor displacement after $t = 1$ ms is predicted to be 5.5 mm.

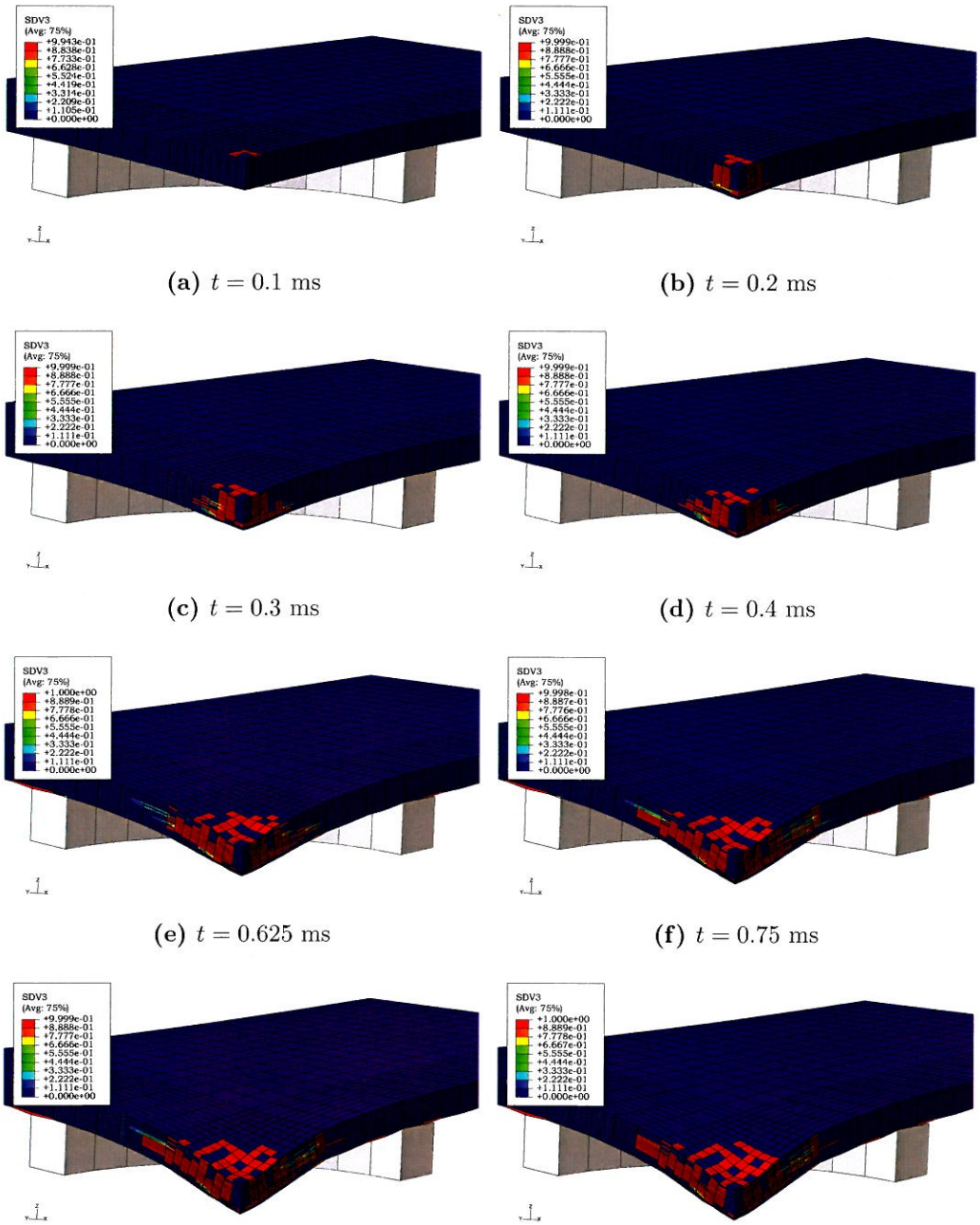

(a) $t = 0.1$ ms **(b)** $t = 0.2$ ms

(c) $t = 0.3$ ms **(d)** $t = 0.4$ ms

(e) $t = 0.625$ ms **(f)** $t = 0.75$ ms

(g) $t = 0.875$ ms **(h)** $t = 1$ ms

Figure 4.9: Predicted delamination using `VUMAT` with $\dot{\boldsymbol{\omega}} \neq \mathbf{0}$

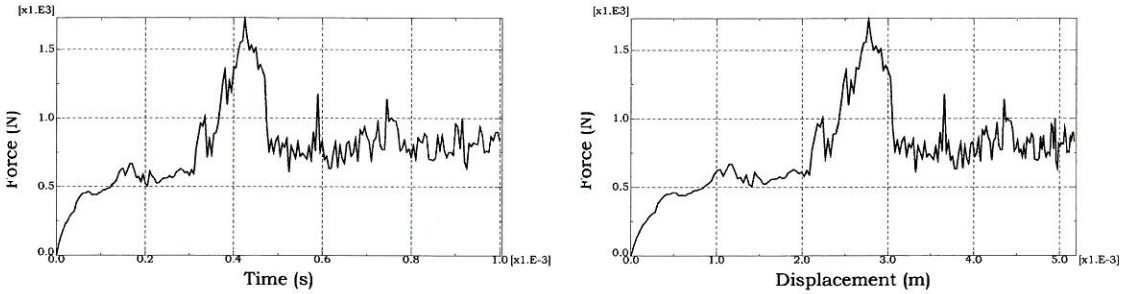

Figure 4.10: Numerically simulated impactor reaction force histories for impact energy $E = 6.5$ J

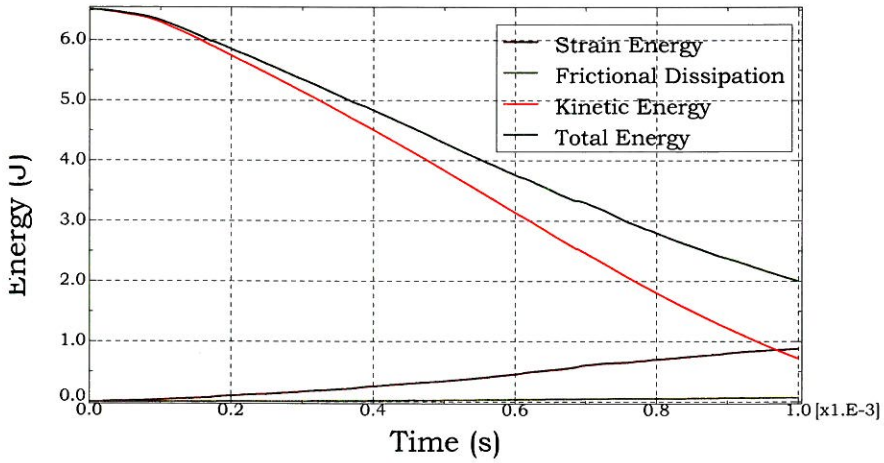

Figure 4.11: Numerically simulated energy histories for impact energy $E = 6.5$ J

During an impact with rebound, such as the one considered here, the impact energy is totally transferred to the laminate. Part of it is accumulated in the form of elastic energy and another part is dissipated in various damage modes or as impactor/laminate and laminate/support friction. Most of the stored energy is recovered and transferred back to the impactor as it bounces away from the laminate. Energy plots obtained from the numerical simulation in Fig. 4.11 shows the variation of the measured energy transferred from the impactor and dissipated energy forms. It appears that energy balance is generally well simulated

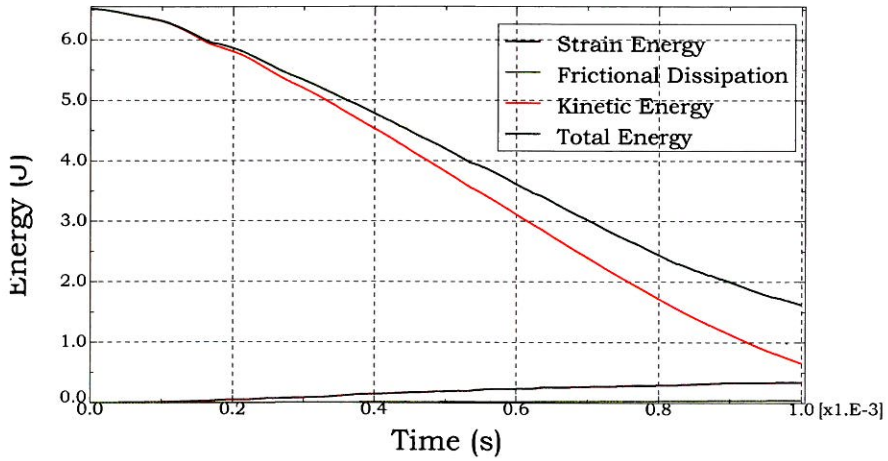

Figure 4.12: Numerically simulated energy histories for a fine mesh for impact energy $E = 6.5$ J

according to the relation

$$\text{Total Energy} = \text{Kinetic Energy} + \text{Total Strain Energy} + \text{Frictional Dissipation} + \text{Viscous Dissipation} + \text{Heat Energy} - \text{other work}$$

At the end of simulation i.e., at $t = 1$ ms the impactor has lost almost all its initial kinetic energy. The difference between the curves representing Total energy and Kinetic energy is a measure of the damage undergone by the laminate. This difference steadily increases and is at its maximum at the end of the simulation implying that maximum damage has occurred till that time.

(c) Localisation effects

As previously pointed out in Section 3.2, mesh regularisation is attempted using only a ply based modelling approach. In order to confirm mesh dependency and capture the localisation effects, two different mesh densities were subjected to identical simulation conditions. Simulation of Hallett's experiment was run with a mesh twice as fine as the original one with the results as presented in Fig. 4.13.

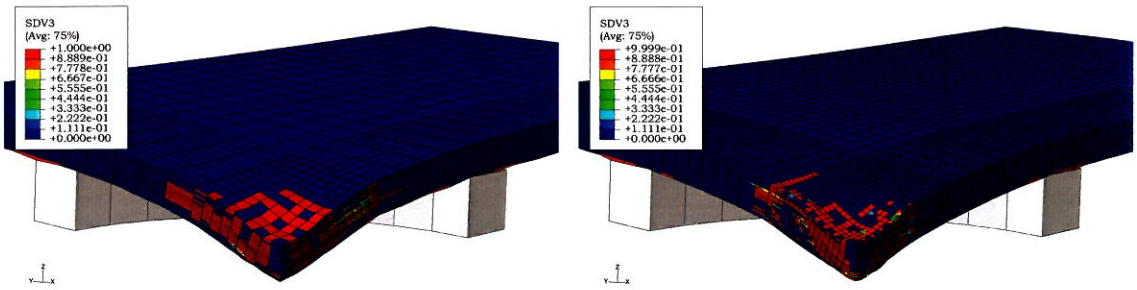

(a) Coarse mesh **(b)** Fine mesh

Figure 4.13: Effect of mesh refinement on predicted damage region with `VUMAT` after $t =$ 1 ms for Hallett's experiment

It can be seen that the final delamination damage pattern is different with the damage zone much contained or in other words localised. However, a plot of the energy history reveals that the energy balance is not violated and is similar to the one presented for a coarse mesh in Fig. 4.11.

4.4 Lopes Experiment

Drop-weight impact tests as devised by the American Society for Testing and Materials (ASTM) and similar to (Airbus Industrie Test Method 1.0010, 1993) were conducted by Lopes (Lopes et al., 2009a) in 2009 (see Fig. 4.14). In the experimental programme, specimens of three different stacking sequence configurations were impacted with energies varying between 5 J and 50 J. The drop heights ranged from 77 cm to 168 cm and the impactor mass was either 951 g, 1.331 kg, 2.441 kg or 4.186 kg, as function of the impact energy. The drop height, H, was chosen to result in a desired impact energy, E_i, related by $H = \frac{E_i}{m_i g}$, where m_i is the impactor mass and g is the acceleration due to gravity (9.81 m/s^2).

In this case, a laminated composite specimen of size 150 x 100 mm^2 was fixed between a steel support measuring 175 x 150 mm^2 and a 10 mm thick steel plate. The 4.368 mm thick specimens consisted of 24 laminated AS4/8552 plies with a nominal

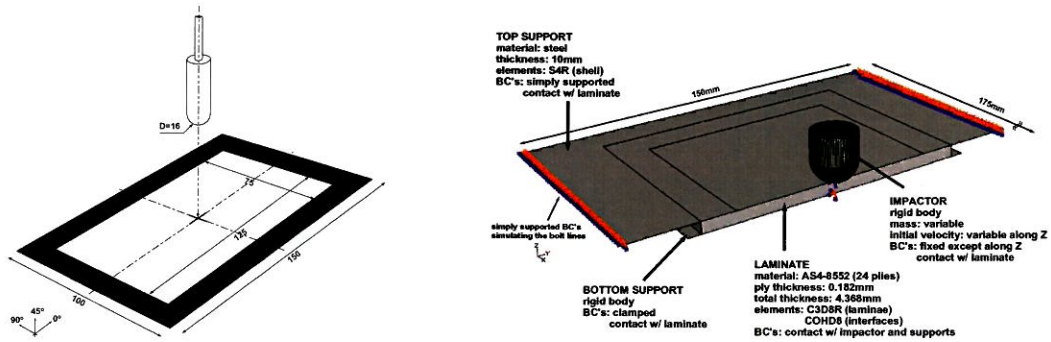

(a) Geometry **(b)** Boundary condition

Figure 4.14: Experimental and simulation set-up (Lopes et al., 2009a,b)

thickness of 0.182 mm each. Both the support and plate had 125 x 75 mm^2 rectangular cuts in the centre, leaving part of the specimens free for impact. The thick steel plate served the purpose of clamps suggested in the standard test procedure to prevent any in-plane movement of the specimen along the supported side areas. The impactor had a similar geometry as described in Section 4.3.

4.4.1 Physical Model

In this simulation, the laminate is modelled as a 24 ply laminate; each ply represented by a section in the model. The laminate model is assigned a $[\pm 45/90/0/45/0_4/-45/0_2]_s$ arrangement of fibre orientation through the section thickness. Available material properties from (Lopes et al., 2009b) were used with rest of the required properties derived using the inter-relationship between them. The Young's modulus and strength properties in the 3-direction were not available and hence, have been assumed. The complete set of material data used in the simulation is presented in Table 4.3. The bottom support, which is considered perfectly rigid and the top steel plate are in contact with the specimen. The top steel plate, simply supported on the outside face, is allowed to deform linearly, whereas the bottom support has a fixed boundary condition applied to it. The impactor mass in the two simulations of 10 J and 20 J impact energy cases was kept as 1.331 kg and 2.441 kg respectively

Property	Value	Units
Young's modulus in the fibre direction E_1	135	GPa
Young's modulus in the transverse direction E_2	9.6	GPa
Young's modulus in the through-thickness direction E_3	9.6	GPa
Poisson's ratio ν_{12}	0.32	
Poisson's ratio ν_{23}	0.487	
Poisson's ratio ν_{13}	0.32	
Shear modulus G_{12}	5.3	Gpa
Shear modulus G_{23}	3.228	Gpa
Shear modulus G_{13}	5.3	Gpa
Tensile strength in the fibre direction X_T	2207	Mpa
Compressive strength in the fibre direction X_C	1531	Mpa
Tensile strength in the transverse direction Y_T	80.7	Mpa
Compressive strength in the transverse direction Y_C	199.8	Mpa
Tensile strength in the through-thickness direction Z_T (assumed)	100	Mpa
Compressive strength in the through-thickness direction Z_C (assumed)	100	Mpa
Shear strength concerning fibre failure S_f	114.5	Mpa
Shear strength concerning matrix cracking S_m (assumed)	80	Mpa
Shear strength concerning delamination S_d (assumed)	80	Mpa
Mass density ρ	1590	kg m^{-3}

Table 4.3: Composite material properties of UD CFRP AS4/8552 (Lopes et al., 2009b)

and the impact velocity was chosen according to the relation $E_i = \frac{1}{2}m_i V_i^2$, where V_i is the velocity of the impactor associated with a mass m_i for a particular energy E_i. Additionally, a force of magnitude $m_i g$ in the vertical direction is applied to the impactor to simulate the gravitational force, where m_i is the impactor mass and g is the acceleration due to gravity (9.81 m/s^2). The analysis was run for a step time of 3 ms as specified in the experimental data by Lopes. The mass of the critical elements around the impact zone was scaled in such a manner so as to limit the overall change in mass of the model to less than 3%.

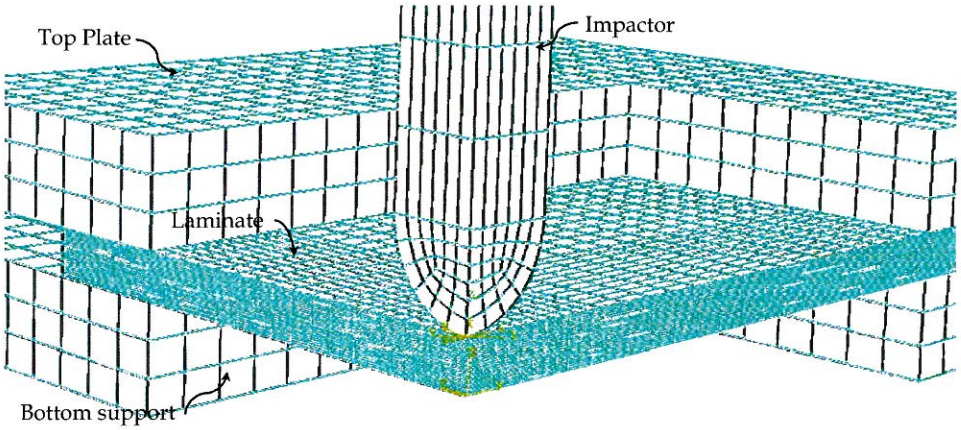

Figure 4.15: Mesh of the plate model for Lopes's experiment

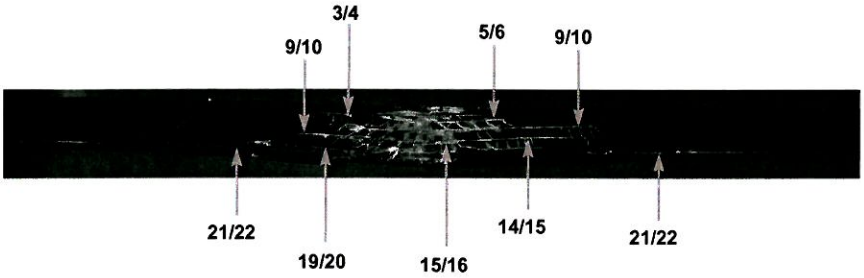

Figure 4.16: Delamination region in Lopes experiment (Lopes et al., 2009a)

4.4.2 Results

Experimental

The results from the experiment of Lopes (Lopes et al., 2009a) are presented in Fig. 4.16, which shows a cut section with the delamination region highlighted by the fluorescent dye. The largest delamination is near the plies farthest away from the impact zone. Lopes (Lopes et al., 2009a) has provided quantitative comparative graphs of reaction force vs impactor tip displacement and reaction force variation over impact time for different impact energies.

Simulation

Results from the simulation of Lopes model indicate the delamination damage prediction as shown in Fig. 4.17. The predicted region is similar to Fig. 4.16. The characteristic damage free region is again predicted right below the impact zone with some delamination in the plies farthest from the impactor.

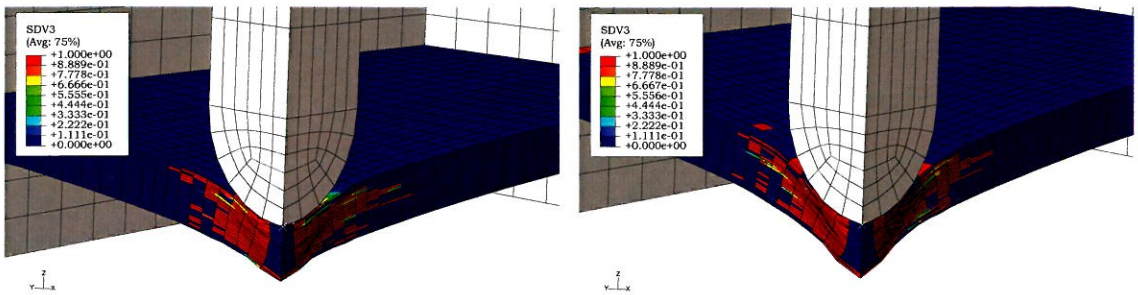

(a) $E_i = 10$ J **(b)** $E_i = 20$ J

Figure 4.17: Predicted delamination damage using `VUMAT` for Lopes impact experiment

Availability of quantitative data in the form of reaction force plots add valuable information to the interpretation of the impact behaviour. Numerically obtained impactor reaction force histories for two different impact energies are presented in Fig. 4.19. For the 10 J energy impact, the peak force is predicted to be around 7 kN which matches quite well with the experimental data but the location in the time scale is different. The peak does match up with the simulation result of Lopes in Fig. 4.18. The initial curve does not quite match up with the experimental curve and this could be attributed to certain shortcoming of the modelling strategy. The impact durations are over predicted hinting that a much increased damage growth is taking place. For the 20 J energy impact, a similar conclusion is drawn. Though the location of the peak force is closer to the experimental value, the initial part of the curve is not presented well. The region around the peak force matches up nicely with the later half sloping towards zero reaction force as the simulation progresses.

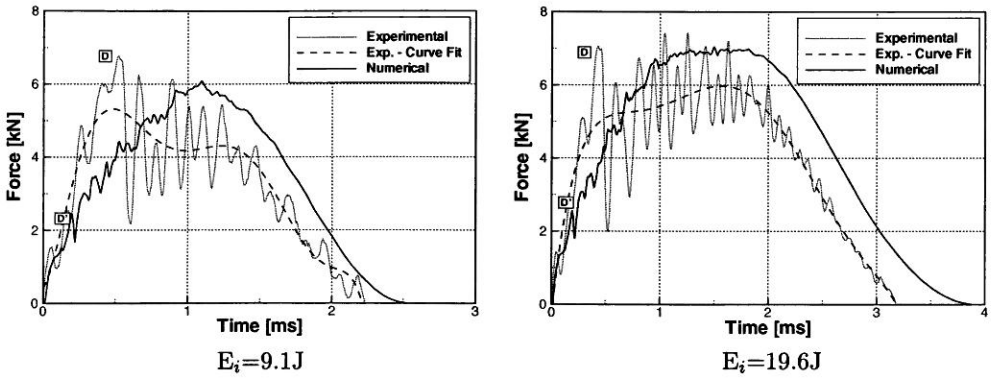

Figure 4.18: Force history plots for different impact energies (Lopes et al., 2009b)

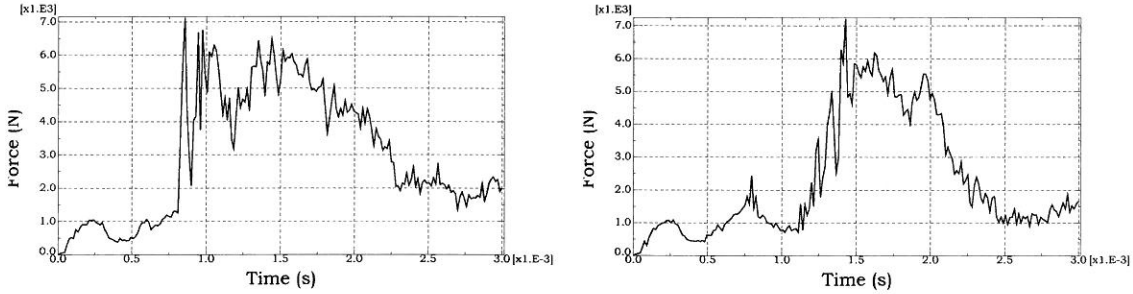

(a) $E_i = 10$ J **(b)** $E_i = 20$ J

Figure 4.19: Numerically simulated impactor reaction force histories for Lopes impact experiment

Fig. 4.21 shows the force vs displacement plot for the simulation corresponding to the 10 J and 20 J impact energies. The mismatch in the plots is quite evident here with an over prediction of the impactor displacement. Again, the peak load location with respect to the tip displacement occurs shifted away. This trend could also indicate a lack of stiffness in the numerically simulated specimen leading to much higher deformations.

The energy plots presented in Fig. 4.22 show the behaviour for two different impact energy cases. It is seen that in the 10 J case the impactor has lost all its kinetic energy and is in the process of bouncing back. The total energy is still not equal to the total

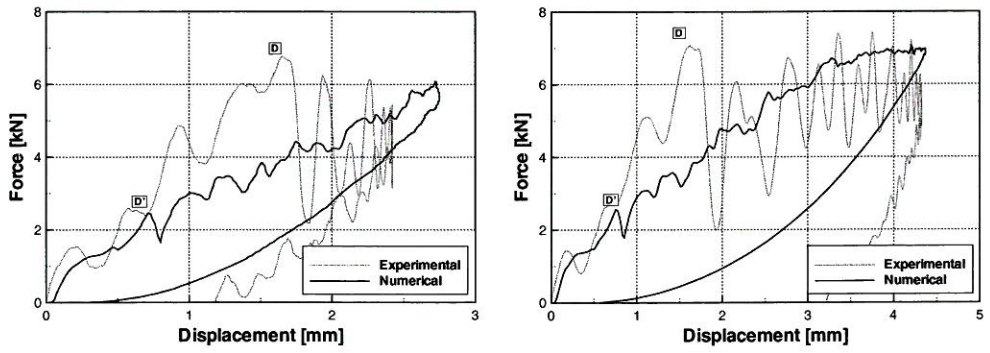

Figure 4.20: Force vs displacement plots for different impact energies (Lopes et al., 2009b)

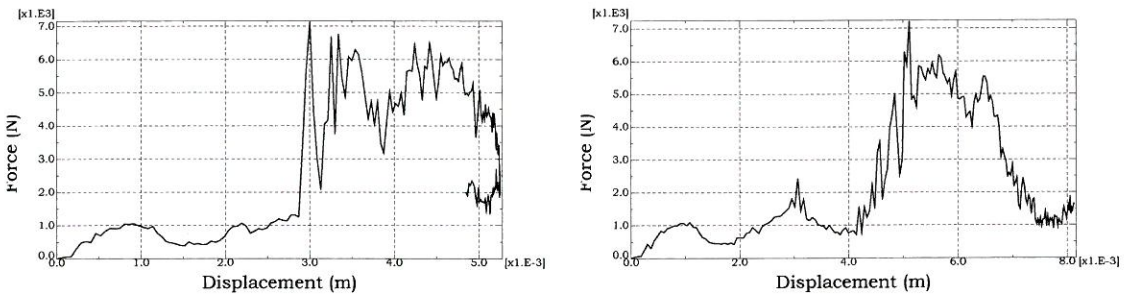

(a) $E_i = 10$ J (b) $E_i = 20$ J

Figure 4.21: Numerically simulated impactor reaction force vs displacement for Lopes impact experiment

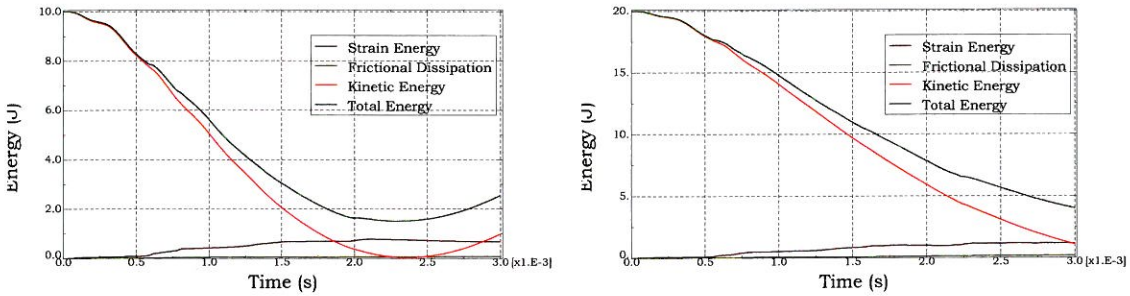

(a) $E_i = 10$ J (b) $E_i = 20$ J

Figure 4.22: Numerically simulated energy histories for Lopes impact experiment

strain energy of the model as additional energy is accumulated in the contact terms. However, for such a scenario it would have been expected to find the occurrence of zero reaction force in the corresponding force history plot at $t = 2.25$ ms. There is still a residual reaction force present. Looking at the 20 J case, it appears that a similar trend would occur if the simulation runs beyond $t = 3$ ms. The energy balance is maintained throughout the simulation, however this aspect of mismatch with the force history plots is noted.

4.5 Summary

In this chapter, low-velocity impact experiments were modelled using the proposed constitutive model. The simulations looked at impact experiments conducted by researchers using aerospace laminate composites at different impact energies. These simulations were conducted in order to verify the constitutive model.

The simulations show that the model is able to predict damage initiation corresponding to the damage modes. Single element tests showed good response when subjected to uniaxial tensile and compressive tests. The strain rate dependency of the model was verified through these tests. The model was capable of predicting damage pattern corresponding to delamination damage similar to the experimental results. Though there exists a certain mesh dependency effect due to the nature of the formulation, use of a mesh size similar to the one used in the literature has yielded comparable results. Delamination was seen to occur in regions where the through thickness stress was high. Delamination criteria normally used tend to predict extensive damage under the impact zone. Only an application of the modified delamination criteria has enabled a more realistic prediction.

The simulation of the highly dynamic impact experiments demonstrate the capability of the model to predict the progressive damage correctly. Dynamic explicit simulations normally suffer from stability problems, which in the present case did not

occur, thus placing confidence in the modelling strategy. Mass scaling was used after lot of trial and error to pull down the simulation time to a reasonable level considering the available resources. It was possible to generate a stable and valid energy response throughout the simulation.

However, comparison of force-time and force-displacement plots suggest that further investigation is required to be carried to understand the reason for discrepancies. The magnitude of reaction force obtained is a good sign that model is capturing some of the effects well, however the location of the peaks in the plots needs to shift to match the experimental observation. A higher deformation of the specimen is observed in the numerical simulations, the root cause of which is not evident clearly. The assumption of material property data in the through-thickness direction might have a role to play in this.

In the final chapter, conclusions are drawn from the present work and development work suggested.

Chapter 5

Conclusions

5.1 Prediction Of Damage Initiation

A three dimensional model for prediction of damage initiation in UD composites using select physically based criteria was used to predict damage, specifically delamination damage under low-velocity impact conditions. The selected failure criteria were stress based and were formulated in a continuum damage mechanics model. Dynamic explicit analysis was carried out using the model. Uniaxial tests on a single element confirmed the validity of model and full scale simulations of actual geometry showed that the model is capable of predicting damage initiation fairly well. The regions of delamination damage were very well represented by the model.

5.2 Prediction of Damage Evolution

The physically based damage initiation criteria were combined with a strain rate dependent evolution model to have a complete capability of predicting progressive damage growth after initiation. The model uses the initiation criteria as dissipation potential to define the damage evolution. Thus, the dissipation potentials comprised only of the stresses that contribute to a particular damage mode. The damage evolution law was dependent on the rate of growth of the damage surface corresponding to

a particular mode. Only damage surface growth outside of the elastic boundary was taken into consideration.

Uniaxial tests on single element confirmed the progressive nature of the model with a small amount of strain captured before complete failure. The strain rate dependency was clearly seen in these tests with higher strain rate leading to a faster damage evolution. The simulations of low velocity impact problems have given an increased confidence in the applicability of the implemented model to such highly dynamic problems. The damage region in general is very well predicted. Consistent energy balance though out the simulation suggests an improvement in the modelling technique compared to previous efforts. However, a consistent observation in the reaction force plots was an over prediction of the impact duration and higher deformation of the specimen corresponding to the peak loads. This discrepancy requires a detailed investigation to find the causes. The possible causes could be either related to the modelling strategy or the limitation of the model itself.

5.3 Future Work

As with every research work, the present effort has provided new learnings and has left many challenges to be addressed in the future. Within the scope of the present work, only a small aspect of numerical modelling related to composites was touched upon. Though new routines incorporating the damage model and improved physical models were generated, lack of model calibration and testing to characterise the strain rate dependency has left much to be desired.

Following suggestions are made in order to improve the current model and better represent the behavior of composites:

- Extensive test data, in particular quasi-static loading cases could be simulated with the model to better characterise the model behavior.

- The present model used initiation criteria based on stresses. Going forward, energy release rate based formulations could be used to better represent the failure and have a more physical meaning. One of the approaches could be to make use of numerical integration techniques with appropriate strength parameters. A related topic would be the introduction of a characteristic length into the formulations to avoid mesh dependency effects.

- The present model worked completely in a continuum damage mechanics framework. However, it is increasingly being appreciated to have a fracture mechanics based approach for delamination damage. This would require development of interface element formulations that can work with the present model. They come with the penalty of high computational cost and hence, care would have to be taken to introduce techniques to bypass this limitation.

- Calibration of the damage directors used in the model is must to enhance the performance of the model. For this extensive experimental or numerical or both would have to be carried out in the future.

Bibliography

[1] Abaqus, I. (2008). *Abaqus Version 6.8.1 User's Manual.*

[2] Airbus Industrie Test Method 1.0010, A. I. (1993). *Fibre reinforced plastics-determination of compression strength after impact. Airbus Industrie Test Method 1.0010.*

[3] Argon, A. S. (1972). Fracture of composites. Volume 1 of *Treatise on material science and technology.* Academic Press, New York.

[4] Benzeggagh, M. L. and M. Kenane (1996). Measurement of mixed-mode delamination fracture toughness of unidirectional glass/epoxy composites with mixed-mode bending apparatus. *Composites Science and Technology 56*(4), 439 – 449.

[5] Boeing Advanced composite tests, B. (1998). *Boeing Specification Support Standard, BSS7260, Rev C.*

[6] Bogetti, T. A., C. P. R. Hoppel, V. M. Harik, J. F. Newill, and B. P. Burns (2004). Predicting the nonlinear response and progressive failure of composite laminates. *Composites Science and Technology 64*(3-4), 329 – 342. Failure criteria in fibre reinforced polymer composites Part C: Additional theories conclusions and recommendations.

[7] Bolotin, V. (1996). Delaminations in composite structures: Its origin, buckling, growth and stability. *Composites Part B-Engineering 27*(2), 129–145.

[8] Bolotin, V. (2001, Sep-Dec). Mechanics of delaminations in laminate composite structures. *Mechanics of Composite Materials 37*(5-6), 367–380.

[9] Brewer, J. and P. Lagace (1988, Dec). Quadratic stress criterion for initiation of delamination. *Journal of Composite Materials 22*(12), 1141–1155.

[10] Budiansky, B. (1983). Micromechanics. *Computers & Structures 16*(1-4), 3 – 12.

[11] Camanho, P., C. Davila, and M. de Moura (2003). Numerical simulation of mixed-mode progressive delamination in composite materials. *Journal of Composite Materials 37*(16), 1415–1438.

[12] Cantwell, W. and J. Morton (1991). The impact resistance of composite materials – a review. *Composites 22*(5), 347 – 362.

[13] Chang, F. and K. Chang (1987, Sep). A progressive damage model for laminated composites containing stress-concentrations. *Journal of Composite Materials 21*(9), 834–855.

[14] Christensen, R. (2009). Failure of fibre laminate composites: Progressive damage and polynomial invariants.

[15] Cuntze, R. G. and A. Freund (2004). The predictive capability of failure mode concept-based strength criteria for multidirectional laminates. *Composites Science and Technology 64*(3-4), 343 – 377. Failure criteria in fibre reinforced polymer composites Part C: Additional theories conclusions and recommendations.

[16] Curiel, J. S., N. Petrinic, and J. Wiegand (2008). A three-dimensional progressive damage model for fibre-composite materials. *Mechanics Research Communications 35*(4), 219 – 221.

[17] Davila, C., P. Camanho, and C. Rose (2005). Failure criteria for FRP laminates. *Journal of Composite Materials 39*(4), 323–345.

[18] Dugdale, D. (1960). Yielding of steel sheets containing slits. *Journal of The Mechanics and Physics of Solids 8*(2), 100–104.

[19] Elder, D. J., R. S. Thomson, M. Q. Nguyen, and M. L. Scott (2004). Review of delamination predictive methods for low speed impact of composite laminates. *Composite Structures 66*(1-4), 677 – 683. Twelfth International Conference on Composite Structures.

[20] Fleck, N. (1997). Compressive failure of fiber composites. Volume 33 of *Advances in Applied Mechanics*, pp. 43 – 117. Elsevier.

[21] Hallett, S. R., W.-G. Jiang, B. Khan, and M. R. Wisnom (2008). Modelling the interaction between matrix cracks and delamination damage in scaled quasi-isotropic specimens. *Composites Science and Technology 68*(1), 80 – 89.

[22] Hashin, Z. (1980). Failure criteria fir unidirectional fibre composites. *Journal of Applied Mechanics 47*(Oct), 329–334.

[23] Hashin, Z. and A. Rotem (1973). Fatigue failure criterion for fibre reinforced materials. *Journal of Composite Materials 7*(Oct), 448–464.

[24] Herakovich, C. T. (1998). *Mechanics of fibrous composites.* John Wiley & Sons, Inc.

[25] Hinton, M. J. and P. D. Soden (1998). Predicting failure in composite laminates: the background to the exercise. *Composites Science and Technology 58*(7), 1001 – 1010.

[26] Hoffman, O. (1967). Brittle strength of Orthotropic materials. *Journal of Composite Materials*.

[27] Hou, J., N. Petrinic, and C. Ruiz (2001). A delamination criterion for laminated composites under low-velocity impact. *Composites Science and Technology 61*(14), 2069–2074.

[28] Kaddour, A., M. Hinton, and P. Soden (2004a). A comparative study of failure theories and predictions for fibre polymer composite laminates: Part (a). In M. Hinton, A. Kaddour, and P. Soden (Eds.), *Failure Criteria in Fibre-Reinforced-Polymer Composites*, pp. 644 – 701. Oxford: Elsevier.

[29] Kaddour, A., M. Hinton, and P. Soden (2004b). Predictive capabilities of nineteen failure theories and design methodologies for polymer composite laminates. part b: Comparison with experiments. In M. Hinton, A. Kaddour, and P. Soden (Eds.), *Failure Criteria in Fibre-Reinforced-Polymer Composites*, pp. 1073 – 1221. Oxford: Elsevier.

[30] Kaddour, A. S., M. J. Hinton, and P. D. Soden (2004c). A comparison of the predictive capabilities of current failure theories for composite laminates: additional contributions. *Composites Science and Technology 64*(3-4), 449 – 476. Failure criteria in fibre reinforced polymer composites Part C: Additional theories conclusions and recommendations.

[31] Kim, R. and A. Crasto (1994). Hygothermal effects on the onset of free-edge delamination in composites. In Drake, K and Bauer, J and Serafini, T and Cheng, P (Ed.), *Moving Forward With 50 Years of Leadership in Advanced Materials - 39th International SAMPE Symposium and Exhibition, Vol 39, Books 1 and 2*, pp. 2935–2947.

[32] Ladeveze, P. and E. LeDantec (1992). Damage modelling of the elementary ply for laminated composites. *Composites Science and Technology 43*(3), 257 – 267.

[33] Lemaitre, J. and J. Chaboche (1978). Phenomenological approach of damage rupture. *Journal de Mecanique Appliquee 2*(3), 317–365.

[34] Liu, K.-S. and S. W. Tsai (1998). A progressive quadratic failure criterion for a laminate. *Composites Science and Technology 58*(7), 1023 – 1032.

[35] Lopes, C., P. Camanho, Z. Gürdal, P. Maimí, and E. González (2009a). Low-velocity impact damage on dispersed stacking sequence laminates. part i: Experiments. *Composites Science and Technology 69*(7-8), 937 – 947.

[36] Lopes, C., P. Camanho, Z. Gürdal, P. Maimí, and E. González (2009b). Low-velocity impact damage on dispersed stacking sequence laminates. part ii: Numerical simulations. *Composites Science and Technology 69*(7-8), 937 – 947.

[37] Maimí, P., P. Camanho, J. Mayugo, and C. Dávila (2007a). A continuum damage model for composite laminates: Part i - constitutive model. *Mechanics of Materials 39*(10), 897 – 908.

[38] Maimí, P., P. Camanho, J. Mayugo, and C. Dávila (2007b). A continuum damage model for composite laminates: Part ii - computational implementation and validation. *Mechanics of Materials 39*(10), 909 – 919.

[39] Matzenmiller, A., J. Lubliner, and R. L. Taylor (1995). A constitutive model for anisotropic damage in fiber-composites. *Mechanics of Materials 20*(2), 125 – 152.

[40] Pagano, N. J. and G. A. Schoeppner (2000). Delamination of polymer matrix composites: Problems and assessment. In A. Kelly and C. Zweben (Eds.), *Comprehensive Composite Materials*, Oxford, pp. 433 – 528. Pergamon.

[41] Pinho, S., L. Iannucci, and P. Robinson (2006a). Formulation and implementation of decohesion elements in an explicit finite element code. *Composites Part A: Applied Science and Manufacturing 37*(5), 778 – 789.

[42] Pinho, S., L. Iannucci, and P. Robinson (2006b). Physically-based failure models and criteria for laminated fibre-reinforced composites with emphasis on fibre kinking: Part i: Development. *Composites Part A: Applied Science and Manufacturing 37*(1), 63 – 73.

[43] Pinho, S., L. Iannucci, and P. Robinson (2006c). Physically based failure models and criteria for laminated fibre-reinforced composites with emphasis on fibre kinking. part ii: Fe implementation. *Composites Part A: Applied Science and Manufacturing 37*(5), 766 – 777.

[44] Pinho, S. T. (2005). Modelling failure of laminated composites using physically-based failure models.

[45] Puck and H. Schurmann (2002). Failure analysis of FRP laminates by means of physically based phenomenological models. *Composite Science and Technology 62*(12-13), 1633–1662.

[46] Quilter, A. (2008). Composites in aerospace applications.

[47] Rosen, B. W. (1965). Fibre composite materials. *Mechanics of composite strengthening, American Society of Metals.*

[48] Tao, J. and C. Sun (1998). Influence of ply orientation on delamination in composite laminates. *Journal of Composite Materials 32*(21), 1933–1947.

[49] Tay, T. and F. Shen (2002). Analysis of delamination growth in laminated composites with consideration for residual thermal stress effects. *Journal of Composite Materials 36*(11), 1299–1320.

[50] Tsai, S. and E. Wu (1971). General theory of strength for anisotropic materials. *Journal of Composite Materials 5*(Jan), 58–&.

[51] Turon, A., P. Camanho, J. Costa, and C. Dávila (2006). A damage model for the simulation of delamination in advanced composites under variable-mode loading. *Mechanics of Materials 38*(11), 1072 – 1089.

[52] Weigand, J. (2009). *3D constitutive model for Impact problems.* Ph. D. thesis, University of Oxford.

[53] Whitney, J. and R. Nuismer (1974). Stress fracture criteria for laminated composites containing stress-concentrations. *Journal of Composite Materials 8*(Jul), 253–265.

[54] Ye, L. (1988). Role of matrix resin in delamination onset and growth in composite laminates. *Composite Science and Technology 33*(4), 257–277.

[55] Zinoviev, P. A., S. V. Grigoriev, O. V. Lebedeva, and L. P. Tairova (1998). The strength of multilayered composites under a plane-stress state. *Composites Science and Technology 58*(7), 1209 – 1223.

Appendix A

VUMAT Routine

```
C ****************comp-vumat-v1.for**********************
C       COMP - VUMAT.V1
C       Version 1.0
C       21/04/2010
C ***********************************************************
C VUMAT SUBROUTINE FOR DAMAGE DETECTION AND EVOLUTION USING
C MATZENMILLER AND CURIEL STRAIN RATE DEPENDENT MODEL FOR
C       LOW VELOCITY IMPACT SIMULATIONS
C Element: C3D8R - solid hexahedral reduced integration element
C (1 gauss point per element)
C ***********************************************************

      subroutine vumat (

C       Read only -
     nblock, ndir, nshr, nstatev, nprops, stepTime, totalTime, dt,
     cmname, props, strainInc, stressOld, stateOld,
C        Write only -
     stressNew, stateNew)

C     implicit none
        include 'vaba_param.inc'
C ***********************************************************

C       ABAQUS VARIABLES:
        integer nblock, ndir, nshr, nstatev, nprops
        real    stepTime, totalTime, dt
        integer errorflag
        Parameter (one = 1.0, four = 4.0, eight = 8.0)
```

```
      Real props(nprops), density(nblock),
      strainInc(nblock,ndir+nshr), stressOld(nblock,ndir+nshr),
      stressNew(nblock,ndir+nshr), stateOld(nblock,nstatev),
      stateNew(nblock,nstatev)
C ************************************************************

C     ARRAY VARIABLES:
      Real  C(6,6), w(6), M(6,6), Cw(6,6), F(6,6,6), q(6,6),
      G1(6,6), G(6,6), e_rate(6), e_rateT(6), InvM(6,6),
      Sum1(6,6), Nabla_g(6,6), phi(nblock,6), w_rate(6),
      w_rateT(6), epsO(nblock,6), epsN(nblock,6)
C ************************************************************

C REAL AND INTEGER VARIABLES
      Real  D, E1, E2, E3, Nu12, Nu21, Nu23, Nu32, Nu31, Nu13,
      Gs12, Gs23, Gs31, X11, X22t, X22c, X33, S12, S23, S31,
      DL, FF1, FF2, MCF1, MCF2, DF1, DF2

      Integer i, k, j, z, l, r, n, v
C ************************************************************
      errorflag = 0

C     MATERIAL PROPERTY ASSIGNMENT
C (Enter in the same order in ABAQUS/EXPLCIT CAE)
      E1 = Props(1)
      E2 = Props(2)
      E3 = Props(3)
      Nu12 = Props(4)
      Nu21 = Props(5)
      Nu23 = Props(6)
      Nu32 = Props(7)
      Nu31 = Props(8)
      Nu13 = Props(9)
      Gs12 = Props(10)
      Gs23 = Props(11)
      Gs31 = Props(12)
      X11 = Props(13)
      X22t = Props(14)
      X22c = Props(15)
      X33 = Props(16)
      S12 = Props(17)
      S23 = Props(18)
      S31 = Props(19)
C -------------------------------------------------------------
C     STIFFNESS MATRIX FOR ORTHOTROPIC MATERIAL
```

```
      D = (1-Nu12*Nu21-Nu23*Nu32-Nu31*Nu13-2*Nu21*Nu32*Nu13)/(E1*E2*E3)

      C(1,1) = (1-Nu23*Nu32)/(E2*E3*D)
      C(2,1) = (Nu12+Nu32*Nu13)/(E1*E3*D)
      C(3,1) = (Nu13+Nu12*Nu23)/(E1*E2*D)
      C(4,1) = 0
      C(5,1) = 0
      C(6,1) = 0

      C(1,2) = (Nu12 + Nu32*Nu13)/(E1*E3*D)
      C(2,2) =  (1- Nu13*Nu31)/(E1*E3*D)
      C(3,2) = (Nu23 + Nu21*Nu13)/(E1*E2*D)
      C(4,2) = 0
      C(5,2) = 0
      C(6,2) = 0

      C(1,3) = (Nu13+Nu12*Nu23)/(E1*E2*D)
      C(2,3) = (Nu23+Nu21*Nu13)/(E1*E2*D)
      C(3,3) = (1-Nu12*Nu21)/(E1*E2*D)
      C(4,3) = 0
      C(5,3) = 0
      C(6,3) = 0

      C(1,4) = 0
      C(2,4) = 0
      C(3,4) = 0
      C(4,4) = Gs12
      C(5,4) = 0
      C(6,4) = 0

      C(1,5) = 0
      C(2,5) = 0
      C(3,5) = 0
      C(4,5) = 0
      C(5,5) = Gs23
      C(6,5) = 0

      C(1,6) = 0
      C(2,6) = 0
      C(3,6) = 0
      C(4,6) = 0
      C(5,6) = 0
      C(6,6) = Gs31
C ------------------------------------------------------------------
C       INITIALISE DAMAGE DIRECTORS
C (Each column corresponds to particular damage mode)
```

```
      do i = 1,6
            do j=1,6
                  q(i,j) = 0
            end do
      end do

C FIBRE RUPTURE
      q(1,1) = 1
C FIBRE BUCKLING
      q(1,2) = 1
C MATRIX CRACKING
      q(2,3) = 1
C MATRIX CRUSHING
      q(2,4) = 1
C DELAMINATION (Tensile)
      q(3,5) = 1
C DELAMINATION (Compressive)
      q(3,6) = 1
C ------------------------------------------------------------------
C     LOOP OVER ELEMENT BLOCKS
            do 100 k = 1, nblock
                  if ( stepTime .eq. 0 ) then
                        do i = 1,6
                              epsO(k,i) = stateOld(k,i+1)
                        end do
                        do i = 1,6
                              epsN(k,i) = strainInc(k,i) + epsO(k,i)
                        end do
C ------------------------------------------------------------------
C     INITIAL STRESS MATRIX: sigma = C * strain
C ------------------------------------------------------------------
                        CALL MATVEC(stressNew(k,:),C,epsN(k,:),6,6)
                  else
                        do i = 1,6
                              w(i) = stateOld(k,i)
                        end do
                        do i = 1,6
                              epsO(k,i) = stateOld(k,i+6)
                        end do
                        do i = 1,6
                              epsN(k,i) = strainInc(k,i) + epsO(k,i)
                        end do
C ------------------------------------------------------------------
C     STRAIN RATE VECTOR
C ------------------------------------------------------------------
                        do i=1,6
```

```
                    e_rate(i) = strainInc(k,i)/dt
                end do
C ---------------------------------------------------------------
C DAMAGED DIAGONAL TENSOR
C ---------------------------------------------------------------
C       Initialize matrix M
                do i = 1,6
                    do j = 1,6
                        M(i,j) =0
                    end do
                end do
C       Compute M= diag[1/(1-w11),1/(1-w22),1/(1-w33),1/(1-w12),1/(1-w23),1/(1-w31)]
                do i = 1, 6
                    M(i,i) = (1-w(i))
                end do
C       Compute damage tensor Cw = M*C
                CALL MATMULT(Cw,M,C,6,6,6)
C ---------------------------------------------------------------
C       NEWSTRESS: StressNew = Cw * epsN
C ---------------------------------------------------------------
                CALL MATVEC(stressNew(k,:),Cw,epsN(k,:),6,6)
C ---------------------------------------------------------------
C       DAMAGE SURFACE IN STRESS SPACE: f
C ---------------------------------------------------------------
C       Initialise F (3rd order tensor: 3rd index points to damage mode)
                do i = 1,6
                    do j = 1,6
                        do v = 1,6
                            F(i,j,v) = 0
                        end do
                    end do
                end do
C       Fiber Rupture
                F(1,1,1) = 1/((1-w(1))**2*X11**2)
                F(4,4,1) = 1/((1-w(4))**2*S12**2)
                F(6,6,1) = 1/((1-w(6))**2*S31**2)
                FF1 = stressNew(k,1)**2*F(1,1,1) +
                    stressNew(k,4)**2*F(4,4,1) +
                    stressNew(k,6)**2*F(4,4,1)
C       Fiber Buckling
                F(1,1,2) = 1/((1-w(1))**2*X11**2)
                F(4,4,2) = 1/((1-w(4))**2*S12**2)
                F(6,6,1) = 1/((1-w(6))**2*S31**2)
                FF2 = stressNew(k,1)**2*F(1,1,2) +
                    stressNew(k,4)**2*F(4,4,2) +
                    stressNew(k,6)**2*F(4,4,2)
```

```
C       Matrix Cracking
                              F(2,2,3)=1/((1-w(2))**2*X22t**2)
                              F(4,4,3)=1/((1-w(4))**2*S12**2)
                              F(5,5,3)=1/((1-w(5))**2*S23**2)
                              MCF1 = stressNew(k,2)**2*F(2,2,3) +
                                     stressNew(k,4)**2*F(4,4,3) +
                                     stressNew(k,5)**2*F(5,5,3)
C       Matrix Crushing
                              F(2,2,4)=1/((1-w(2))**2*X22c**2)
                              F(4,4,4)=1/((1-w(4))**2*S12**2)
                              F(5,5,4)=1/((1-w(5))**2*S23**2)
                              MCF2 = (one/four)*stressNew(k,2)**2*F(4,4,4) +
                                     one/four)*stressNew(k,2)*X22c*F(4,4,4) -
                                     stressNew(k,2)*sqrt(F(2,2,4)) +
                                     stressNew(k,4)**2*F(4,4,4)
C       Delamination (Tensile)
                              F(3,3,5)=1/((1-w(3))**2*X33**2)
                              F(5,5,5)=1/((1-w(5))**2*S23**2)
                              F(6,6,5)=1/((1-w(6))**2*S31**2)
                              DF1 = stressNew(k,3)**2*F(3,3,5) +
                                     stressNew(k,5)**2*F(6,6,5) +
                                     stressNew(k,6)**2*F(6,6,5)
C       Delamination (Compressive)
                              F(3,3,6)=1/((1-w(3))**2*X33**2)
                              F(5,5,6)=1/((1-w(5))**2*S23**2)
                              F(6,6,6)=1/((1-w(6))**2*S31**2)
                              DF2 = (-eight*stressNew(k,3)**2 + stressNew(k,5)**2 +
                                     stressNew(k,6)**2)*F(6,6,6)
                              DL = -(sqrt(one/eight*
                                     (stressNew(k,5)**2+stressNew(k,6)**2)))
C ---------------------------------------------------------------
C       Compute G = CwT * F * Cw (3rd order tensor in strain space)
C ---------------------------------------------------------------
                              do z = 1,6
C       Partial Product Matrix G1 = F * Cw
                                 CALL MATMULT(G1,F(:,:,z),Cw,6,6,6)
C       G Matrix
                                 CALL MATMULT(G, transpose(Cw),G1,6,6,6)
                                 do p=1,6
                                        do r=1,6
                                               Sum1(p,r)=G(p,r)+G(r,p)
                                        end do
                                 end do
C ---------------------------------------------------------------
C       GRADIENT TO STRAIN SURFACE: Nabla_g = epsN * (transpose(G) + G)
C ---------------------------------------------------------------
```

```
                                    CALL MATVEC(Nabla_g(z,:),Sum1,epsN(k,:),6,6)
                                end do
C ---------------------------------------------------------------------
C       DAMAGE GROWTH FUNCTION: phi = epsN_rate * Nabla_g
C ---------------------------------------------------------------------
                                CALL MATVEC(phi(k,:),Nabla_g,e_rate,6,6)
C       Correction for direction of damage growth; no growth if damage surface is
C not tresspassed
                                do l = 1,6
                                    if (phi(k,l).lt.0)then
                                        phi(k,l) = 0
                                    end if
                                end do
C       Associating normal stress direction with growth function
                                do j = 1,3
                                    if (stressNew(k,j).gt.0) then
                                        phi(k,2*j) = 0
                                    else
                                        phi(k,2*j-1) = 0
                                    end if
                                end do
C ---------------------------------------------------------------------
C       DAMAGE RULE: w_rate = phi * q
C ---------------------------------------------------------------------
                                CALL MATVEC(w_rate,q,phi(k,:),6,6)
C ---------------------------------------------------------------------
C       DAMAGE INITIATION
C ---------------------------------------------------------------------
C       Fibre failure
                                if (stressNew(k,1).ge.0) then
                                    if (FF1.lt.one) then
                                        w_rate(1) = 0
                                    end if
                                else
                                    if (FF2.lt.one) then
                                        w_rate(1) = 0
                                    end if
                                end if
C       Matrix cracking and Crushing
                                if (stressNew(k,2).ge.0) then
                                    if(MCF1.lt.one) then
                                        w_rate(2) = 0
                                    end if
                                else
                                    if (MCF2.lt.one) then
                                        w_rate(2) = 0
```

```
                                    end if
                                end if
C       Delamination (Tensile and compressive)
                                if (stressNew(k,3).ge.0) then
                                    if (DF1.lt.one) then
                                        w_rate(3) = 0
                                    end if
                                else
                                    if (stressNew(k,3).ge.DL) then
                                        if(DF2.lt.one) then
                                            w_rate(3) = 0
                                        end if
                                    else
                                        w_rate(3) = 0
                                    end if
                                end if
C ---------------------------------------------------------------
C       DAMAGE EVOLUTION
C ---------------------------------------------------------------
                                do i = 1,6
                                  w_rateT(i) = w_rate(i)*dt
                                end do
C       Increment damage variable
                                do i = 1,6
                                    w(i) = w(i) +  w_rateT(i)
                                end do
C       Max limit for damage variable (To avoid by zero)
                                do n = 1,6
                                    if (w(n).ge.1) then
                                        w(n) = 0.99
                                    else if (w(n).lt.0) then
                                        w(n) =0
                                    end if
                                end do
C ---------------------------------------------------------------
C       UPDATE STATE VARIABLES
C ---------------------------------------------------------------
                                do i =1,6
                                    stateNew(k,i) =w(i)
                                end do
                                do i = 1,6
                                    stateNew(k,i+6) =epsN(k,i)
                                end do
                            end if

100     end do
```

```
      return
      end subroutine vumat

C ************************************************************
C       Subroutine MATMULT
C PERFORMS MATRIXxMATRIX PRODUCT A=B*C, B(NA,NB), C(NB,NC)
C ------------------------------------------------------------
      SUBROUTINE MATMULT(A,B,C,NA,NB,NC)
      IMPLICIT NONE
            INTEGER I,J,X,NA,NB,NC
            REAL A(NA,NC),B(NA,NB),C(NB,NC)
            DO I=1,NA
                  DO J=1,NC
                        A(I,J) = 0
                              DO X=1,NB
                                    A(I,J)=A(I,J)+B(I,X)*C(X,J)
                              ENDDO
                  ENDDO
            ENDDO
      END SUBROUTINE MATMULT
C ------------------------------------------------------------
C       Subroutine MATVEC
C PERFORMS MATRIXxVECTOR PRODUCT v=A*u, A(NA,NB), u(NB)
C ------------------------------------------------------------
      SUBROUTINE MATVEC(v,A,u,NA,NB)
      IMPLICIT NONE
            INTEGER I,J,NA,NB
            REAL v(NA),A(NA,NB),u(NB)
            DO I=1,NA
                  v(I)=0
                        DO J=1,NB
                              v(I)=v(I)+A(I,J)*u(J)
                        ENDDO
            ENDDO
      END SUBROUTINE MATVEC
C ------------------------------------------------------------
C ************************************************************
C       ****************************** END ********************
C ************************************************************
```